The evolution of gene expression in seasonal environments

Shuichi N. Kudo[1], Yuka Ikezaki[2], Junko Kusumi[3], Hideki Hirakawa[4,5], Sachiko Isobe[4,6], Akiko Satake[2]*

1. Graduate School of Systems Life Sciences, Kyushu University, Fukuoka 819-0395, Japan
2. Department of Biology, Faculty of Science, Kyushu University, Fukuoka 819-0395, Japan
3. Department of Environmental Changes, Faculty of Social and Cultural Studies, Kyushu University, Fukuoka 819-0395, Japan.
4. Kazusa DNA Research Institute, 2-6-7 Kazusa-kamatari, Kisarazu, Chiba 292-0818, Japan
5. Graduate School of Bioresource and Bioenvironmental Sciences, Kyushu University, Fukuoka 819-0395, Japan
6. Graduate School of Agricultural and Life Sciences, The University of Tokyo, Tokyo, 113-8657, Japan

*Corresponding author: Akiko Satake

Email: satake.akiko.269@m.kyushu-u.ac.jp

Abstract

The biological activities of organisms are closely linked to seasonality. Phenology, the temporal orchestration of biological activities, is governed by gene expression, yet the evolutionary dynamics underlying seasonal gene expression remain unclear. To investigate these dynamics, we compared genome-wide expression dynamics (molecular phenology) in four dominant evergreen Fagaceae species in Asia (*Quercus glauca*, *Q. acuta*, *Lithocarpus edulis*, and *L. glaber*), using leaf and bud tissues over two seasonal cycles. We assembled high-quality reference genomes, identifying 11749 single-copy orthologous genes. Seasonal transcriptomic profiling of these orthologous genes revealed highly conserved gene expression across species in winter when temperatures fall below ~10°C. Rhythmic gene expression with significant periodic oscillations was more prevalent in buds (51.9%) than in leaves (40.6%), with most rhythmic genes (78.4–92.0%) exhibiting annual periodicity, while a smaller fraction (1.2–11.9%) followed half-annual cycles. The seasonal peaks of rhythmic genes were highly synchronized across species in winter but diverged during the growing season, reflecting species-specific timing of leaf flushing and flowering. These findings suggest that the four species share a common molecular calendar in winter, which constrains the evolution of gene expression under seasonal environments.

Introduction

Fundamental biological processes, such as growth, mortality, and reproduction, rarely remain constant over time; instead, they exhibit pronounced variation in response to seasonal environmental changes (Fretwell, 1972). This temporal organization of a series of biological activities, known as phenology, plays a critical role in the evolution of life histories in response to seasonal fluctuating environments (Forrest and Miller-Rushing, 2010; Morellato et al., 2013; Piao et al., 2019; Schwartz, 2013). Phenology is regulated by the coordinated expression of genes that enable organisms to exhibit essential functions at the appropriate times (Kudoh, 2016; Satake et al., 2024a, 2022). However, gene expression dynamics underpinning seasonal responses in organisms remain not fully understood.

To explore the evolution of gene expression, transcriptome analyses are widely employed to compare transcript profiles across organs, sexes, species, and developmental stages within a given environment. Such studies have been conducted in mammals (Brawand et al., 2011; Cardoso-Moreira et al., 2019; Naqvi et al., 2019), *Drosophila* (Lemos et al., 2005; Nuzhdin et al., 2004), and Tanzanian cichlids (El Taher et al., 2021), providing key insights into the evolutionary dynamics of gene expression and its central role in shaping phenotypic diversity. These studies have revealed that gene expression profiles tend to be more conserved across species within the same tissue, whereas the evolutionary rate of gene expression varies among organs. In mammals, for instance, nervous tissue exhibits a slower rate of gene expression change compared to the testis (Brawand et al., 2011; Cardoso-Moreira et al., 2019; Naqvi et al., 2019), suggesting the

presence of tissue-specific functional constraints that influence the evolution of gene expression.

In addition to tissue-dependent constraints, seasonal environmental changes may play a crucial role in shaping the evolution of gene expression, particularly by influencing the temporal coordination of gene expression under natural conditions. Gene expression responses to certain seasons may be more resistant to change, whereas in other seasons, divergence in gene expression timing across species may occur, contributing to temporal niche differentiation. Despite its potential importance, the influence of seasonal environmental fluctuations on the gene expression evolution remains poorly understood, largely because most transcriptomic analyses have been conducted under tightly controlled laboratory conditions.

To investigate the evolution of gene expression in seasonal environments, we performed a molecular phenology analysis and phenological observation of leaf flushing and flowering in Fagaceae tree species, which are widely distributed across the Northern Hemisphere, with its center of diversity in subtropical Southeast Asia (Hipp et al., 2020; Kremer et al., 2012; Manos et al., 2001; Zhou et al., 2022). Molecular phenology refers to transcriptome analysis conducted under natural fluctuating conditions (Komoto et al., 2024; Kudoh, 2016; Nagano et al., 2019; Satake et al., 2023) and provides a valuable framework for studying gene–environment interactions and their role in orchestrating the temporal biological functions essential for adaptation to environmental fluctuations (Satake et al., 2022). In this study, we selected four evergreen Fagaceae species—two *Quercus* species (*Q. glauca* and *Q. acuta*) and two *Lithocarpus* species (*L. edulis* and *L. glaber*)—that co-occur in the same locality in Japan. *Q. glauca*, *L. edulis* and *L. glaber* inhabit nearly identical environment, while *Q. acuta* is restricted to the high-altitude regions with slightly colder environment compared to the other three species. Leaf flushing and flowering phenology vary across species, with *Q. glauca* and *Q. acuta* flowering in early spring, almost simultaneously with leaf flushing, *L. edulis* flowering in late spring, and *L. glaber* flowering in autumn, approximately one to two months after leaf flushing. This setting enabled us to compare seasonal gene expression profiles across species with diverse phenology, both within and between genera, under nearly identical environmental fluctuations. By assessing and comparing seasonal transcriptomic dynamics across Fagaceae species, our study provides new insights into the evolution of gene expression and adaptation to seasonal natural environments.

Results

Genome assemblies of *Q. glauca* and *L. edulis*. To quantify transcript abundance of non-model Fagaceae species, we first constructed reference genomes for *Q. glauca*, as a representative of genus *Quercus*, and *L. edulis,* as a representative of genus *Lithocarpus* (Fig. 1A). To obtain high-quality chromosome-level reference genomes, we conducted a hybrid genome assembly for the HiFi reads and the high-throughput chromosome conformation capture (Hi-C) reads (Table S1).The resultant scaffolds were 867.7 and 835.7 Mb and consisted of 797

and 750 scaffolds including 12 chromosome-level scaffolds with contig N50 of 71.7 Mb and 68.8 Mb for *Q. glauca* and *L. edulis*, respectively (Table S1). Approximately 94.8% and 97.2% of the final assemblies were assigned to 12 pseudochromosomes of *Q. glauca* and *L. edulis*, respectively (Fig. 1B). The number of chromosome-scale scaffolds were identical to the known numbers in other *Quercus* (Zoldos et al., 1999) and *Lithocarpus* species (Liu et al., 2023). The genomes were estimated to contain 39758 and 34059 protein-coding genes (33947 and 30246 genes were annotated within 12 chromosomes), covering 98.3% and 95.0% of complete Benchmarking Universal Single Copy Orthologs (BUSCO) genes (eudicots_odb10) for *Q. glauca* and *L. edulis*, respectively. The genome sizes of *Q. glauca* and *L. edulis* were estimated to be 891.2 Mb and 868.7 Mb, respectively, using KmerGenie (Chikhi and Medvedev, 2014) and GenomeScope2 (Ranallo-Benavidez et al., 2020).

Overall, the abundance and distribution of protein-coding genes, GC content, and repeat sequences (Fig. 1C, D*;* Table S1) and syntenic structure (Fig. 1B) were similar between *Q. glauca* and *L. edulis*. This pattern of synteny conservation appears to be broadly shared across Fagaceae, except for the genus *Fagus*, which shows a distinct genome structure (Ikezaki et al., 2025). The homology between different chromosomes within the genome suggests that small-scale segmental duplications likely occurred, as previously proposed (Chen et al., 2014). Using OrthoFinder2 (Emms and Kelly, 2019), we clustered genes from the two newly assembled genomes into orthologous groups. We identified 13427 single-copy orthologs, enabling pairwise comparisons between species (Fig. 1E).

Seasonal gene expression dynamics. To characterize the evolution of seasonal gene expressions, we generated a total of 483 transcriptome profiles every four weeks over two years using leaf and bud tissues from *Q. glauca*, *Q. acuta*, *L. edulis*, and *L. glaber* during 2021–2023. Reads from the two *Quercus* species were mapped to the newly constructed *Q. glauca* reference genome, achieving a mean mapping rate of 92.6 ± 2.2% and 88.6 ± 2.3% for *Q. glauca* and *Q. acuta*, respectively. Similarly, reads from the two *Lithocarpus* species were mapped to the newly constructed *L. edulis* reference genome, with a mean mapping rate of 89.3 ± 2.7% and 84.3 ± 5.4% for *L. edulis* and *L. glaber*, respectively. The number of reads uniquely mapped on the reference genome was 19.9 million reads per sample, on average. We used single-copy orthologous genes for further analyses because these genes exhibited significantly higher average expression levels than multi-copy genes (Steel-Dwass test, $p < 0.05$; Fig. 1F, G). Among the single copy orthologous genes, we excluded genes with low expression levels (mean of Reads Per Kilobase (RPK) across samples for each species < 1) and normalized the transcript count data using the GeTMM method (Smid et al., 2018). This process resulted in a high-quality expression dataset for 11749 genes (Fig. S1A). For further analyses, we used the mean expression levels across three biological replicates (three individuals per species), except for *L. edulis*, where only one individual was available. We confirmed that expression patterns of individual genes were highly consistent across all the three biological replicates (Fig. S2) in *Q.*

glauca (Pearson's correlation r = 0.947), *Q. acuta* (r = 0.948) and *L. glaber* (r = 0.948).

To gain an initial overview of gene expression dynamics in a seasonal environment, we assessed the relative magnitude of seasonal variation in expression levels for each gene by calculating the standard deviation divided by the mean for each gene (σ_i/μ_i) and compared it to the overall variation across all genes in the genome (σ_g/μ_g) (Fig. S1B). A prior study using 3025 yeast RNA-seq experiments reported that the dynamic range of individual genes across experiments was considerably smaller than the overall genomic variation under laboratory conditions (Zrimec et al., 2021). Consistently, our results demonstrate that despite substantial seasonal fluctuations in environmental conditions (Fig. S3), individual gene expression remains relatively conserved. On average, the magnitude of genome-wide variation was 15.8 times greater than the seasonal variation observed for individual genes (Fig. S1B).

To assess the similarity of gene expression profiles across tissues, species, and seasons, we performed a hierarchical clustering of seasonal transcriptome profiles from leaf and bud tissues across four species and identified five distinct clusters (cluster L1, L2, B1–B3) according to the Elbow method (Fig. 2A; Fig. S4A; Dataset S1). Transcriptional profiles first grouped into leaves (cluster L1 and L2) and buds (cluster B1–B3), irrespective of seasons and species (Fig. 2A), except that newly flushed leaf samples were grouped closely with buds (Fig. 2A; Fig. S5). Within the leaf cluster, transcriptome profiles were first clustered by genus and then by species in *Lithocarpus* (cluster L1; Fig. 2A). In contrast, samples from *Quercus* species formed a mixture of two species (cluster L2; Fig. 2A). Notably, the winter samples of *Q. acuta*, collected during periods of low mean temperatures, were distinctly separated from those collected in other seasons (cluster L2; Fig. 2A). Within the bud cluster, transcriptome profiles were predominantly grouped by season—winter (cluster B3; November to February, with the exception of a March sample from *L. edulis*; Dataset S1) versus the other growing seasons (cluster B1 and B2; March to November; Dataset S1)—and subsequently organized by genus and species. This suggests that the winter season exerts a stronger influence on gene expression in buds than phylogenetic relationships. We confirmed the robustness of our findings to differences in sampling periods between *Quercus* and *Lithocarpus* species by reanalyzing expression data limited to common sampling periods (Fig. S6). Even when using only the data from this shared period, the clustering patterns were consistently reproduced. To assess whether the higher-elevation site of *Q. acuta* introduced confounding environmental effects, we reanalyzed the data after excluding this species. Hierarchical clustering still revealed that winter bud samples formed a distinct cluster regardless of species identity (Fig. S7), consistent with our original findings.

To assess the biological relevance of the clusters identified, we tested whether the temperatures and photoperiod at the time of sample collection differed significantly among the clusters. Within the bud cluster, transcriptional profiles in the winter cluster (cluster B3) were associated with significantly lower temperatures—approximately below 10 °C—compared to those in other seasons

(Fig. 2B; Fig. S8A). In contrast, no such temperature-related distinction was evident within the leaf cluster (Fig. 2B). Additionally, photoperiods were markedly shorter in the winter cluster in buds (Fig. S8B). These findings suggest that the buds of the four species exhibit a conserved transcriptional response to environmental cues, namely cold temperatures and short photoperiods, characteristic of the winter season. To further investigate the relationships among all samples, we conducted a principal component analysis (PCA). The first principal component (PC1) clearly separated samples by tissue type, while the second (PC2) and the third principal component (PC3) gradually differentiated winter samples from those collected during other seasons (Fig. S9).

To investigate seasonal expression dynamics of each gene, we conducted hierarchical clustering on the transcriptional dynamics of 11749 genes and identified five distinct gene sets characterizing different transcriptional modes (gene set I–V; Fig. 2C, D; Fig. S4B; Dataset S2). Gene set I exhibited predominant expression in buds, with seasonal peaks during summer, whereas gene set II was primarily expressed in leaves, highlighting clear tissue-specificity (Fig. 2C, D). Gene sets III and V demonstrated genus-specific expression patterns, with higher expression levels observed in *Lithocarpus* and *Quercus*, respectively (Fig. 2C, D). In contrast, gene set IV was expressed during winter across both leaf and bud tissues (Fig. 2C, D).

Detection of rhythmic genes. To identify genes revealing seasonal expression dynamics and determine the period and seasonal peaks in gene expression, we applied the RAIN algorithm (Thaben and Westermark, 2014). This approach enabled us to detect genes with rhythmic expression (hereafter rhythmic genes) and analyze their periods and phases (peak months). Our analysis revealed that 44.6–58.8% of genes in bud tissues and 33.9–45.9% in leaf tissues exhibited significant rhythmic expression across species (Fig. S10A; Dataset S3). Notably, bud tissues demonstrated a higher proportion of rhythmic genes, with 51.9% across four species on average, compared to 40.6% in leaf tissues (Fig. S10A).

Among the rhythmic genes, the majority (78.4–92.0%) exhibited annual periodicity, with a period of 12 ± 1 month observed across species and tissues (Fig. 3A, B, Dataset S3). Additionally, hundreds of genes (1.2–11.9%) displayed half-annual periodicity (6 ± 1 month) with these genes being most frequently observed in the bud samples of *L. edulis* (Fig. 3A, B). The fraction of genes exhibiting other periodicities was relatively small (5.7–14.1%; Fig. 3A, B). Based on the observed period distributions, we classified genes with periods within the range of 8–16 months as exhibiting annual periodicity (96.0%) and those with periods shorter than 8 months as having half-annual periodicity (4.0%), accounting for detection noise (Fig. S10A). Rhythmic genes with longer periods (>17 months) were also identified, although their periodicity may be less reliable due to the limited number of time points. Many genes with annual periodicity were shared across all species, including 1280 genes in leaves and 1894 genes in buds (Fig.

S10B). In contrast, most genes exhibiting half-annual periodicity were species-specific, with no genes shared among all the species (Fig. S10C).

Peak month distribution of rhythmic genes and intra-genus and inter-genera comparison. To determine the seasonal timing of gene expression peaks, we focused on genes with annual or half-annual periodicity and visualized the density and direction of these peaks throughout the year using a circular histogram (Fig. 3C, D; Dataset S3). On average, 34.9% and 41.3% of annual rhythmic genes peaked in winter (December–February) in leaf and bud samples, respectively. Additionally, another peak corresponding to or occurring slightly after leaf flushing and flowering events was observed, with its timing varying by species: April in *Q. glauca* (15.6%), July in *Q. acuta* (15.3%), June in *L. edulis* (16.0%), September in *L. glaber* (18.1%), for leaf tissues (Fig. 3C). Similar peaks corresponding to leaf flushing or flowering were also detected in bud samples, occurring approximately one to two months earlier than in leaf samples (Fig. 3D). For genes with half-annual periodicity, the majority (63.2 ± 4.8%) exhibited expression peaks both in spring (March–May) and autumn (September–November) in both tissues (Fig. S10D; Dataset S3), with the exception of *L. glaber*, an autumn flowering species. Interestingly, *WRKY22*, a transcription factor regulating ethylene biosynthesis and senescence (Zhu et al., 2024), exhibited half-annual periodicity in *L. glaber* (Fig. S10*E*). In addition, *SNF1-RELATED PROTEIN KINASE REGULATORY SUBUNIT GAMMA 1* (*KINγ1*), a subunit of SNF1-related kinase (*SnRK*) involved in stress response such as starvation (Emanuelle et al., 2016), showed two distinct peaks in *Q. glauca* and *L. edulis*, occurring in both summer (July) and winter (January) (Fig. S10E). This result suggests that both summer and winter pose stressful conditions for these species.

To compare the peak month of gene expression with annual periodicity across species, we quantified the number of genes within each peak combination for both intra-genus (Fig. 4A) and inter-genera species pairs in buds (Fig. 4B) and leaves (Fig. S11A, B). During winter, a large number of genes exhibited highly synchronized expression peaks across species, with high pairwise Pearson's correlation coefficients observed (Fig. 4A, B). In contrast, the peak timing of gene expression from spring to autumn varied across species, aligning with differences in leaf flushing and flowering times (Fig. 4A, B). Some genes exhibited pronounced divergence, showing negative Pearson's correlation coefficients (< -0.3) between species. Notably, the number of such genes was larger in inter-genera comparisons (11–77 genes; Fig. 4B) than in intra-genus comparisons (4–12 genes; Fig. 4A). A similar pattern was observed in leaf samples (Fig. S11A, B). When comparing seasonal expression peaks between tissues, the majority of genes were synchronously activated in winter in both tissues (Fig. S11C). During spring to summer, slight variations in seasonal expression peaks were observed among tissues (Fig. S11C).

We quantified the degree of divergence in seasonal gene expression patterns across species by calculating the peak month differences between two species, where one species exhibits an expression peak in the given month. We

defined the molecular phenology divergence index (*D*) for each month by quantifying the proportion of genes with peak month differences greater than 2 months between two species, relative to the total number of genes with expression peaks in that month. From spring to autumn, the mean of *D* over all species pairs in buds ranged from 0.47 to 0.66, but it declined sharply during winter, reaching a minimum of 0.12 in January in buds (Nemenyi test, $p < 0.05$; Fig. 4C). A similar trend was observed in leaf samples, with another trough in summer (Fig. S11D). This seasonal trend remained consistent even after excluding *Q. acuta*, which was sampled from a slightly cooler environment than the other three species, from the analysis (Fig. S12), indicating that the observed patterns are not drive by environmental differences associated with elevation. The values of *D* were not consistently smaller in inter-genera pairs compared to intra-genus pairs. These findings suggest that there is a seasonal constraint in gene expression in which the degree of molecular phenology divergence is not constant but varies significantly across seasons, with the least divergence occurring in winter.

Phylogenetic constraints in the evolution of seasonal gene expression. We next investigated whether phylogenetic relationship influences the evolution of seasonal gene expression by calculating pairwise Pearson's correlations of seasonal expression for each gene across all species pairs (Dataset S4). The median of Pearson's correlation coefficients across all genes were significantly higher between species within the same genus compared to those between species from different genera in both leaves (Steel-Dwass test, $p < 0.05$; Fig. S13A; Fig. S14) and buds (Steel-Dwass test, $p < 0.05$; Fig. 5A; Fig. S14). The intra-genus comparison in genus *Lithocarpus* exhibited the highest correlation in their seasonal gene expression, despite their notable differences in flowering phenology, with *L. edulis* flowering in spring and *L. glaber* in autumn. In contrast, the intra-genus comparison in genus *Quercus* resulted in a relatively low correlation in their gene expression regardless of relatively similar phenology in leaf flushing and flowering. This difference may be attributed to environmental factors, as *Q. acuta* is the only species found in the high-altitude study site with colder climates compared to the other three species.

Rhythmic genes exhibited more conserved expression patterns than arrhythmic genes in both tissues (Fig. 5*A*; Fig. S13A). In particular, genes with seasonal expression peaks in winter showed high correlation across species in both tissues (Fig. 5B; Fig. S13B). The proportion of rhythmic genes with annual periodicity declined as the mean correlation coefficient across species decreased, with a more rapid decline observed for genes peaking in winter compared to those with peak expression during the growing seasons (Fig. 5B; Fig. S13B). Additionally, the mean absolute difference in seasonal gene expression dynamics was significantly smaller between species within the same genus than between species from different genera in both tissues (Fig. S15A, B). The relationship between the mean absolute difference and the proportion of rhythmic genes was less clear compared to that of the mean correlation coefficient (Fig. S15C, D). These findings suggest that, in addition to seasonal constraints, the overall

331 dynamics of seasonal gene expression are also shaped by phylogenetic
332 constraints.
333
334 **Functional annotation of genes with conserved or divergent expression**
335 **across species.** To functionally annotate genes with conserved or divergent
336 expression across species, we extracted genes with the top and bottom 5% based
337 on the distribution of mean correlation (Fig. 5B; Fig. S13B) and conducted Gene
338 Ontology (GO) enrichment analysis. GO analysis revealed that the top 5% of genes
339 in leaves were associated with photosynthesis, while those in buds were linked to
340 cell fate determination (Fig. S16A; Dataset S5). The gene with the highest
341 correlation in leaves was *STRESS RESPONSE SUPPRESSOR1* (*STRS1*; mean
342 of pairwise correlation = 0.91; Fig. 5C), a DEAD-box RNA helicase previously
343 reported to enhance tolerance to abiotic stresses such as cold (Kant et al., 2007).
344 In buds, the most highly correlated gene was the histone deacetylase *HDA19*
345 (mean of pairwise correlation = 0.93; Fig. 5C), which plays a key role in
346 environmental stress responses through histone modification and chromatin
347 remodeling (Chen and Wu, 2010). These findings suggest that genes associated
348 with photosynthesis during the growing season and stress responses during winter
349 exhibit highly conserved seasonal expression patterns across species.
350 The bottom 5% of genes were predominantly associated with DNA
351 replication and cell division in leaves (Fig. S16B), aligning with the divergent leaf
352 phenology observed (Fig. 3B). In contrast, GO terms related to immune response
353 were weakly enriched in buds (Fig. S16B). Notably, we identified MADS-box genes
354 linked to floral transition among the bottom 5% of genes: *BROTHER OF FT AND*
355 *TFL1* (*BFT*) in leaves (mean of pairwise correlation = -0.094) and *FRUITFULL*
356 (*FUL*) in buds (mean of pairwise correlation = -0.069). *BFT*, a floral repressor (Yoo
357 et al., 2010), was expressed in autumn in the spring-flowering species *L. edulis*
358 and in spring in the autumn-flowering species *L. glaber* leaves (Fig. 5D).
359 Meanwhile, *FRUITFULL* (*FUL*), a positive regulator of floral transition (Smaczniak
360 et al., 2012), was expressed in spring in *L. edulis* and in autumn in *L. glaber* (Fig.
361 5D), mirroring the timing of flowering. In *Q. glauca* and *Q. acuta*, *FUL* was
362 expressed in winter (Fig. 5D), nearly out of phase with their expressions in
363 *Lithocarpus* species. These results suggest that genes involved in reproductive
364 processes exhibit species-specific divergence in expression patterns in response
365 to seasonal environmental changes.
366
367 **Relating seasonal gene expression divergence to sequence divergence.** If
368 divergence of seasonal timing of gene expression is related to selective constraint,
369 we would expect a correlation between sequence divergence patterns and the
370 divergence in seasonal expression peaks. To explore the relationship between the
371 divergence of seasonal gene expression and protein sequence evolution, we
372 calculated synonymous (dS) and non-synonymous substitution rates (dN) and their
373 ratio (dN/dS) for each gene using coding sequences from newly assembled
374 genomes of *Q. glauca* and *L. edulis*. We first confirmed that the highly expressed
375 genes evolve more slowly by identifying a significant negative correlation between

evolutionary rate (dN/dS) and mean of the gene expression (r = -0.21, p = 1.8 × 10^{-118} for dN/dS; Fig. S17A; Dataset S6). This finding aligns with previous studies in yeasts, mammals, and plants (Drummond et al., 2005; Gaut et al., 2011; Liao and Zhang, 2006; Yang and Gaut, 2011). By targeting the genes that exhibited annual periodicity across both species and tissues, we examined the relationship between these evolutionary measures and peak month differences in seasonal gene expression between species ($\Delta\varphi$) in leaves and bud tissues using linear regression. Assessment of the significance of the regression coefficient using a *t*-test revealed that genes with smaller peak month differences between species exhibited lower values of dN/dS in buds (p =2.6 × 10^{-2}) and marginally lower values of dN/dS in leaves (p = 5.7 × 10^{-2}). The lower values were also found in dN in both leaves (p = 8.1 × 10^{-3}) and buds (p = 7.8 × 10^{-3}), whereas no significant trend was observed for dS in both tissues (Fig. 5E; Fig. S17B, C; Dataset S6). We further investigated whether the association between the divergence in seasonal expression peaks and sequence divergence patterns varies between genes expressed in winter and in the growing season. We classified genes that exhibited annual periodicity across both species and tissues into four groups based on their expression peak timing (winter or growing seasons) and tissue specificity (leaves or buds) and compared the extent of protein sequence divergence across these groups. We found no significant differences in dN/dS (Kruskal Wallis test, p = 2.8 × 10^{-1}; Fig. S17*D*; Dataset S6) between genes expressed in winter in both tissues and those in growing seasons. The same result was observed even when focusing only on genes with conserved peaks (peak month difference < 2), with no significant differences in dN/dS between these gene sets (Kruskal Wallis test, p = 3.5 × 10^{-1}; Fig. S17E; Dataset S6). These results suggest that coding-sequence variation is unlikely to be the primary driver of seasonal gene expression patterns.

Discussion

A central goal in biology is to unravel the molecular basis of phenotypic evolution, with gene expression serving as a fundamental driver of this process. In this study, we investigated the impact of seasonal environmental fluctuations on the evolution of gene expression and its relationship with phenological traits in four dominant *Fagaceae* tree species in forest ecosystems. We found that gene expression profiles were more resistant to change during winter compared to the growing season, indicating the presence of a seasonal constraint on the evolution of gene expression. This constraint becomes particularly pronounced in buds during winter when temperatures fall below approximately 10°C (Fig. 2B). This temperature threshold aligns with previous findings, where winter-specific transcript profiles were reported at temperatures below 8.7–11.3°C in cherry trees (Miyawaki - Kuwakado et al., 2024), 11.3°C in ever-green *Fagaceae* (Satake et al., 2023), and 10.5°C in perennial *Arabidopsis* (Aikawa et al., 2010). These results suggest the presence of a conserved mechanism for gene expression regulation under low-temperature environments across different species. The greater conservation of gene expression patterns in buds compared to leaves across species may be attributed to their functional role protecting essential meristematic tissues,

421 including the shoot apex and leaf and flower primordia. Additionally, buds likely
422 play a crucial role in maintaining common physiological functions necessary for the
423 resumption of growth in spring. This functional consistency may impose
424 evolutionary constraints on gene expression, contributing to its conservation
425 across species.

426 It is intriguing to compare the seasonal constraints identified in this study
427 with developmental constraints in gene expression evolution, where evolutionary
428 conservation and variation across developmental stages during the life cycle have
429 been observed, such as in the early conservation model and the developmental
430 hourglass model (Fig. S18A)(Irie and Kuratani, 2011; Lotharukpong et al., 2024;
431 Quint et al., 2012). Previous studies have demonstrated that certain developmental
432 stages exhibit remarkably similar gene expression patterns (Drost et al., 2016;
433 Kalinka et al., 2010; Levin et al., 2016). Our findings highlight that such highly
434 similar gene expression patterns are observed during the winter season (Fig.
435 S18B), suggesting that a common physiological state is essential for enduring
436 harsh winter conditions. This seasonal constraint on gene expression evolution
437 may have the potential to limit temporal niche partitioning at the phenotypic level
438 and slow species divergence rates in seasonal environments (Cleland and
439 Wolkovich, 2024; Kubo and Iwasa, 1996). Although completely disentangling the
440 effects of developmental stages and seasonal changes on gene expression is
441 challenging when using molecular phenology data collected from natural
442 environments, the observation that species with different phenology—i.e., different
443 developmental timing in seasonal environments—exhibit convergent gene
444 expression patterns during winter underscores the profound influence of winter
445 environmental conditions on the evolution of gene expression. Future research is
446 needed to elucidate the mechanisms driving the establishment of such conserved
447 gene expression patterns, including the dynamic reorganization of chromatin
448 architecture in response to cold (Fischl et al., 2020; Nishio et al., 2020; Zhang et
449 al., 2023).

450 We found that the evolution of coding-sequences was only weakly
451 correlated with the divergence of seasonal peaks in gene expression across
452 species. To understand the evolutionary mechanism underlying the seasonal
453 constraint on gene expression that results in similar expression patterns during
454 winter, an important future direction is to explore the evolution of non-coding
455 sequences that modulate gene expression levels in response to seasonal
456 environmental changes. Regulatory variation has been recognized as a major
457 driver of evolutionary innovation (Prud'homme et al., 2007; True and Haag, 2001).
458 Recent deep learning studies utilizing genome and transcriptome data from yeast
459 and humans have highlighted the significance of co-evolution between coding and
460 non-coding sequences in shaping gene expression levels (Zrimec et al., 2021,
461 2020). Understanding how seasonal environments drive the co-evolution of coding
462 and regulatory sequences, as well as the divergence of molecular phenology and
463 its phenological outputs, will require expanding analyses to a broader range of
464 species. Such efforts will facilitate the development of predictive models for
465 evolutionary processes influenced by seasonal dynamics. Comparison of

466 molecular phenology across wide climatic zones, including both tropical and
467 temperate zones, will also be effective to identify key genes for the phenological
468 response to on-going climate change.
469

470 Materials and Methods

471 Sample collection for genome sequencing

472 To construct genomes of *Q. glauca* and *L. edulis*, we collected approximately 5g
473 of fresh leaves from one individual in spring, respectively. We shipped these
474 samples to Dovetail Genomics, LLC (Scotts Valley, CA, USA) where Dovetail Staff
475 performed DNA extraction, library preparation, sequencing, and assembly steps.
476

477 Genome sequencing and assembly

478 DNA extraction was performed using the QIAamp DNA Mini Kit (Qiagen,
479 Germantown, MD, USA) using the manufacturer's recommended protocol. Mean
480 fragment length of the extracted DNA was 60 kbp for *Q. glauca* and 65 kbp for *L.*
481 *edulis*. DNA samples were quantified using Qubit 2.0 Fluorometer (Life
482 Technologies, Carlsbad, CA, USA). The library preparation, sequencing and
483 scaffolding were carried out by Dovetail Genomics (California, USA) according to
484 their standard genome assembly pipeline (https://dovetailgenomics.com/). The
485 PacBio SMRTbell library (~20kb) for PacBio Sequel was constructed using
486 SMRTbell Express Template Prep Kit 2.0 (PacBio, Menlo Park, CA, USA) using
487 the manufacturer's recommended protocol. The library was bound to polymerase
488 using the Sequel II Binding Kit 2.0 (PacBio) and loaded onto PacBio Sequel II.
489 Sequencing was performed on PacBio Sequel II 8M SMRT cells. PacBio CCS
490 reads were used as an input to Hifiasm1 v0.15.4-r347 with default parameters. For
491 *Q. glauca*, we also generated sequence data using PacBio Revio. BLASTn results
492 of the contigs obtained by Hifiasm assembly against the NCBI's NT database were
493 used as input for blobtools2 v1.1.1 and contigs identified as possible contamination
494 were removed from the assembly. Finally, purge_dups3 v1.2.5 was used to
495 remove haplotigs and contig overlaps.
496

497 Assembly scaffolding with HiRise

498 A proximity ligation library was generated by the Dovetail's Omni-C technique,
499 followed by sequencing on an Illumina HiSeqX platform. Chromatin was fixed in
500 place in the nucleus with formaldehyde before extraction
501 (https://dovetailgenomics.com/wp-content/uploads/2021/09/Omni-C-Tech-
502 Note.pdf). Fixed chromatin was digested with DNase I, and the fragmented
503 chromatin ends were repaired and biotinylated to adapters followed by proximity
504 ligation. Crosslinks were then reversed, the DNA purified, and the biotin
505 subsequently removed. The DNA library was prepared and sequenced to produce
506 2 × 150 bp paired-end reads (around 30× coverage). The Omni-C technology uses
507 a sequence-independent endonuclease which provides even, unbiased genome
508 coverage. The input *de novo* assembly and Omni-C library reads were used as
509 input data for HiRise, a software pipeline designed specifically for using proximity
510 ligation data to scaffold genome assemblies (Putnam et al., 2016). The Omni-C

511 library sequences were aligned to the contigs assembled by Hifiasm using bwa (Li
512 and Durbin, 2009). The separations of Omni-C reads from paired-end mapped
513 within the contigs were analyzed by HiRise to produce a likelihood model for
514 genomic distance between paired-end reads, and the model was used to identify
515 and break putative misjoins, to score prospective joins, and make joins above a
516 threshold.
517
518 **Sample collection for RNA sequencing**
519 To monitor the genome-wide gene expression profiles, we collected leaf, bud, and
520 flower samples from four Fagaceae species, *Q. glauca*, *Q. acuta*, *L. edulis* and *L.*
521 *glaber*, every four weeks for two years (October 2019 to October 2021 for the
522 *Lithocarpus* species and April 2021 to April 2023 for the *Quercus species*) across
523 Fukuoka and Saga prefectures in Kyushu, Japan. We targeted three individuals,
524 and each sample was collected from three branches per individual, except for *L.*
525 *edulis*. Given the consistent expression patterns observed among individuals in a
526 previous study (Satake et al., 2023), we focused on only one individual for *L. edulis*.
527 Study sites for *Q. glauca* is the biodiversity reserve on the Ito campus of Kyushu
528 University (33º35′ N, 130º12′ E, 20 to 57 m a.s.l). *L. edulis* and *L. glaber* were
529 studied at the Imajuku Field Activity Center (33º33′ N, 130º16′ E, 84 to 111 m a.s.l).
530 The Imajuku and Ito Campus study sites, located only 7.3 km apart, experience
531 nearly identical temperature conditions. *Q. acuta* was monitored in Sefuri
532 mountains (33º26′ N, 130º22′ E, 970 to 974 m a.s.l), a higher-altitude, cooler site.
533 Environmental data from Ito Campus and the Imajuku Field Activity Center were
534 obtained from the Japan Meteorological Agency, while data from Sefuri Mountain
535 were collected using a logger installed at the sampling site. Additionally, to assess
536 the potential impact of different sampling periods between the *Lithocarpus* and
537 *Quercus* species on the gene expression analysis, we conducted an additional
538 year of sampling for *L. edulis* and *L. glaber*, collecting leaf and bud samples from
539 November 2021 to November 2022, and used the samples collected within the
540 same period for all the four species (May 2021 to November 2022).
541 Samples for RNA-seq were taken from the sun-exposed crown
542 (approximately 2–5 m from the ground) using long pruning shears from 11:30 to
543 12:30 h. For each sample, 0.2–0.4 g of tissue was preserved in a 2 ml microtube
544 containing 1.5 ml of RNA-stabilizing reagent (RNAlater; Thermo Fisher Scientific,
545 Waltham, MA, USA) immediately after harvesting. The samples were transferred
546 to the laboratory within 2 hr after sampling, stored at 4°C overnight and then stored
547 at −80°C until RNA extraction. During transport to the laboratory, the samples were
548 kept in a cooler box with ice to maintain a low temperature.
549
550 **RNA extraction and RNA-seq analysis**
551 RNA was extracted independently from bud and leaf samples of each tree. Total
552 RNA of the leaf sample was extracted in accordance with the method described in
553 a previous study (Miyazaki et al., 2014). Total RNA of the bud sample was
554 extracted using the PureLink™ Plant RNA Reagent (Thermo Fisher Scientific,
555 Waltham, MA, USA) and subsequently processed with DNase using the TURBO

556 DNA-free kit™ (Thermo Fisher Scientific) according to their protocols and purified
557 using the RNeasy Plant Mini Kit (Qiagen, Hilden, Germany) according to its RNA
558 cleanup protocol. RNA integrity was examined using the Agilent RNA 6000 Nano
559 kit on a 2100 Bioanalyzer (Agilent Technologies), and the RNA yield was
560 determined using a NanoDrop ND-2000 spectrophotometer (Thermo Fisher
561 Scientific). Five to six micrograms of RNA extracted from each sample were sent
562 to Hangzhou Veritas Genetics Medical Institute Co., Ltd., where a cDNA library
563 was prepared with a NEBNext Ultra II RNA Library Prep Kit for Illumina, and 150
564 base paired-end transcriptome sequencing of each sample was conducted using
565 an Illumina NovaSeq6000 sequencer (Illumina).
566 The quantification of gene expression followed a three-step process. First,
567 quality filtering was performed using the fastp v0.23.2 with default options: phred
568 quality ≥15, the maximum number of N base in one read = 5 (Chen et al., 2018).
569 Second, RNA-seq reads were mapped to the reference genome using STAR
570 v2.7.10b (Dobin et al., 2013). Third, RNA-seq reads were quantified using RSEM
571 v1.3.1 (Li and Dewey, 2011). We excluded the genes with low expression level
572 using the threshold, the value of mean Reads Per Kilobase (RPK) < 1 for each
573 species. Then, we further normalized the expression level using the value of Gene
574 length corrected Trimmed Mean of M-values (GeTMM) (Smid et al., 2018) using
575 an R package "edgeR" v3.42.4. For the downstream analysis we calculated the
576 mean expression levels of GeTMM of each gene across multiple individuals and
577 transformed them to $\log_2$(GeTMM+1). To confirm that the effect of the difference
578 in sampling period is negligible, we added the RNA-Seq data of *L. edulis* and *L.*
579 *glaber* collected from December 2021 to December 2022. We extracted the same
580 genes in the existing data that curated based on the mean RPK values across two-
581 year sampling periods. Then we further normalized the expression level using
582 GeTMM.
583
584 **Genome annotation**
585 The RNA-seq reads of *Q. glauca* (8 samples obtained by a previous study (20)
586 collected from May to December 2017; GEO's accession number: GSE211384)
587 and *L. edulis* (20 samples covering leaf, bud and flower tissues collected in
588 January, April, July, and November 2021) were respectively mapped against the
589 scaffolds of *Q. glauca* and *L. edulis* obtained by HiRise with HISAT2 v2.1.0 (Kim
590 et al., 2019). The bam files generated by the mappings and amino acid sequences
591 of the 9 species obtained from NCBI (*Castanea mollissima*: GCA_000763605.2
592 (NCBI's accession number), *Q. lobata*: GCF_001633185.1, *Q. robur*:
593 GCF_932294415.1, *Q. suber*: GCF_002906115.1, *Carpinus fangiana*:
594 GCA_006937295.1, *Carya illinoinensis*: GCF_018687715.1, *Juglans macrocarpa*
595 × *J. regia*: GCF_004785595.1, *Juglans regia*: GCF_001411555.2, *Morella rubra*:
596 GCA_003952965.2) were used for ab initio gene prediction by Braker2 v2.1.6
597 (Brůna et al., 2021), and the genes with highest-score were selected to exclude
598 splicing variants. In parallel, the gene models were respectively constructed in *Q.*
599 *glauca* and *L. edulis* by GeMoMa v1.7.1 (Keilwagen et al., 2019) with RNA-seq
600 reads and amino acid sequences used for the gene prediction in Braker2, and the

genes with highest-score were selected to exclude splicing variants. The duplicated genes between Braker2 and GeMoMa were excluded by GFFcompare v0.11.2 (Pertea and Pertea, 2020). The remaining genes were searched against UniProtKB (Bateman et al., 2025) by DIAMOND v2.0.5 (Buchfink et al., 2014) in 'more-sensitive' option with E-value $\leq 10^{-20}$ and identity ≥25%. Next, gene expression analysis was performed by Salmon v1.4.0 (Patro et al., 2017), and the genes with TPM values >0.1 were considered as expressed. The orthologous genes were searched against EggNOG (Hernández-Plaza et al., 2023) using eggNOG-mapper v2.1.8 (Cantalapiedra et al., 2021) with E-value $\leq 10^{-10}$. The genes were searched against protein sequences of *Castanea mollissima* (Accession: GCA_000763605.2), *Quercus lobata* (GCF_001633185.2), and *Arabidopsis thaliana* (Araport11 (Krishnakumar et al., 2015)) by BLASTp v2.13.0 (Camacho et al., 2009) with E-value $\leq 10^{-20}$. According to these similarity searches, the genes whose product names contain keywords related to transposable elements (TEs) were categorized into TE. The genes having similarity hits and being expressed by Salmon were classified into high-confidence (HC) genes, while remaining genes were categorized into low-confidence (LC) genes. The genes categorized into HC were used for further analyses.

Genome synteny analysis

To investigate the syntenic relationship between *Q. glauca* and *L. edulis*, we first performed an all-vs-all BLASTp search of the protein sequences, using a cut-off E-value of 10^{-5}. Collinearity blocks within and between the genomes were then identified using MCScanX (Wang et al., 2012) based on the results of the BLASTp searches. Finally, the collinearity blocks were visualized using SynVisio (https://synvisio.github.io).

Illumina short-read sequencing and library preparation

For genome size estimation and phylogenetic reconstruction, we also generated short-read sequencing of *Q. glauca*, *Q. acuta*, *L. edulis*, and *L. glaber.* DNA extraction was performed using a modified version of the method described previously (Satake et al., 2024b). The DNA samples were sent to Macrogen Inc. (Republic of Korea) for sequencing on the Illumina HiseqX platform (Illumina, San Diego, CA, USA). DNA was sheared to around 500 bp fragments in size using dsDNA fragmentase (New England BioLabs, Ipswich, MA, USA). Library preparation was performed using the NEBNext Ultra II DNA Library Prep Kit (New England BioLabs) according to the manufacturer's protocol, and the libraries were individually indexed with the NEBNext Multiplex Oligos for Illumina (New England BioLabs) by PCR. The quality and quantity of each amplified library were analyzed using the Bioanalyzer 2100 (Agilent Technologies, Santa Clara, CA, USA), the High Sensitivity DNA kit (Agilent Technologies), and the NEBNext Library Quant Kit for Illumina (New England BioLabs).

Genome size estimation

The genome size of *Q. glauca* was estimated by GenomeScope2 v2.0 (Ranallo-Benavidez et al., 2020) using *k*-mer frequency plot obtained by kmc v3.2.4 (Kokot et al., 2017) with *k*-mer size 61 against the HiFi reads. We also used pair-end short reads for genome size estimation of *Q. glauca* and confirmed that resulted estimates were not different. For *L. edulis*, paired-end short reads from four individuals were merged and quality-trimmed using fastp v0.23.2 (Chen et al., 2018). The genome size was then estimated using KmerGenie (Chikhi and Medvedev, 2014) with a k-mer size of 55 applied to the trimmed reads.

Phylogenetic reconstruction

We constructed a phylogenetic tree using an alignment-free method (Fan et al., 2015) based on short-read data from *Q. acuta* and *L. glaber* and genome assembly data from *Q. glauca* and *L. edulis*. Additionally, genomic data for *Fagus sylvatica* was obtained from beechgenome.net (Mishra et al., 2022) and included as an outgroup. Due to the large volume of short-read data for *Q. acuta* and *L. glaber* (18 Gb each), we randomly subsampled half of the reads. Bootstrap values were estimated through 100 resampling of the k-mer table.

Identification of orthologs

The prediction of orthogroups was based on a BLASTp all-against-all comparison of the protein sequences (E-value < 10^{-5}) of 5 Fagaceae species: *L. edulis*, *Q. glauca*, *Q. robur*, *Fagus sylvatica* and *Juglans regia*. Clustering was conducted with OrthoFinder2, using version 2.2.6 for BLAST data generation and version 2.5.5 for orthogroup determination (Emms and Kelly, 2019). The genomic data of *Q. robur* and *J. regia* were downloaded from NCBI (dhQueRobu3.1 and Walnut 2.0), while *F. sylvatica* data were sourced from beechgenome.net (Mishra et al., 2022). Since the *F. sylvatica* dataset contained numerous predicted transposable elements (TEs), we re-annotated genes using three databases—EggNOG5 (EggNOG-mapper), Pfam35.0 (HMMER v3.3.2), and UniRef90_2023_0628 (DIAMOND v2.1.8.162)—and excluded genes identified as TEs in at least one database. In total, we identified 26692 orthogroups and focused on single-copy orthogroups after filtering out genes mapped outside the 12 chromosomes. This resulted in a final dataset of 11749 genes for further analysis (Data S2).

Hierarchical clustering and principal component analysis (PCA)

To assess the similarity of the genome-wide transcriptional profiles across orthologous genes and 483 samples collected in different seasons, we performed hierarchical clustering using the monthly time series data of 11749 orthologous genes from October 2019 to April 2023. For each orthologous gene, there were 26 or 27 time points, with three individuals each for *Q. glauca*, *Q. acuta*, *L. glaber* and one individual for *L. edulis*. We calculated the mean expression levels of each orthologous gene across three individuals in each species and subsequently normalized the values by adjusting the mean to zero and the standard deviation to one. We performed hierarchical clustering using the Ward method and the Euclidian distance using the pheatmap function in R (v 1.0.12). To determine the

number of the clusters, we calculated Within-Cluster-Sum of Squared Error (WSS) and determined the number of clusters as an elbow point of it (Fig. S4). To assess the seasonal expression dynamics of 11749 orthologous genes, we also performed PCA of the gene expression profiles from all samples using the prcomp function in R (v 4.3.1).

Identification of genes with rhythmic expression

To identify genes with rhythmic expression and determine the period and peak month of gene expression, we applied the RAIN algorithm (Thaben and Westermark, 2014) using the rain function in R (v 1.34.0). We set the following settings: deltat = 1, period = 12, period.delta = 11, peak.border = (0,1), nr.series = 1, method= "independent", na.rm= T , adjp.method = "ABH". Based on the results of the RAIN analysis, we identified genes with significant periodicity using a Benjamini-Hochberg (BH) adjusted *q*-value threshold of < 0.01. Since the period length and peak month in the RAIN output are expressed in terms of the number of time points, we converted them into months using the sampling span (four weeks) and sampling dates. Subsequently, we categorized the rhythmic genes into three categories based on the period length T (in months): “half-annual” ($0 \leqq T < 8$), “annual” ($8 \leqq T \leqq 16$), and “long” ($T > 16$).

Calculation of Pearson’s correlation coefficient across species

To quantify the similarity of seasonal gene expression pattern across species, we calculated pairwise Pearson’s correlations of seasonal expression for each gene across all the species pairs. For species within the same genus, the monitoring period was identical, allowing direct comparison. On the other hand, the monitoring periods differed between *Quercus* and *Lithocarpus* species: *Q. glauca* and *Q. acuta* were monitored from May 2021 to April 2023, while *L. edulis* and *L. glaber* were monitored from October 2019 to October 2021 (Fig. S3). To ensure comparable time series data for inter-genera comparisons, we extracted the time series from *Q. glauca* and *Q. acuta* spanning May 19, 2021, to November 2, 2022, and from *L. edulis* and *L. glaber* spanning May 13, 2020, to October 20, 2021, for correlation analysis. The mean absolute differences for each gene across all the species pairs were also calculated in a similar manner.

Molecular phenology divergence index (*D*)

To quantify the seasonal difference of peak month divergence across species, we defined the molecular phenology divergence index (D) for each month t and species pair A-B as the proportion of genes that peak in month t in the reference species A but exhibit a peak month difference ($\Delta\varphi$) greater than two months in species B using following formula:

$$D := \frac{\#\ \text{Genes with peak month } t \text{ in species A and } t \pm \Delta\phi(\geq 2) \text{ in species B}}{\#\ \text{Genes with peak month } t \text{ in species A}}.$$

Gene Ontology (GO) enrichment analysis

First, we assigned GO terms for each gene in *Lithocarpus* and *Quercus* genomes based on the annotation data of *Arabidopsis thaliana* orthologs downloaded from PLAZA Database (http://bioinformatics.psb.ugent.be/plaza/). Then, GO enrichment analysis was conducted using the GOstats (Falcon and Gentleman, 2007) function in R (v 2.66.0) with the following settings: ontology = BP, pvalueCutoff = 0.05, conditional = TRUE, and testDirection = over. The universe gene set was defined as genes associated with GO terms common to both of the genomes. Genes without annotated GO terms were removed from the universe set, and those with differing GO term annotations between the two genomes were also excluded. The BH adjusted *q*-values were calculated from the *p*-values generated by GOstats to account for multiple testing.

Phenology measurement: leaf unfolding and flowering

To compare seasonal changes in genome-wide gene expression profiles with phenology, we conducted observations of leaf unfolding and flowering phenology on the three terminal branches of each of the three individuals used for gene expression monitoring. Leaf unfolding was defined as the stage where both the entire leaf blade and the leaf stalk were visible (Fig. S5). Flowering was defined as the stage where either male or female flowers were visible (Fig. S5). We subsequently plotted the proportion of branches exhibiting leaf unfolding and flowering. The data are provided in Dataset S2.

Estimation of protein-coding sequence divergence

Pairwise distances for non-synonymous (dN) and synonymous (dS) substitutions, as well as the dN/dS ratio, were estimated for each orthologous gene pair between *L. edulis* and *Q. glauca* using codeml (PAML 4.0)(Yang, 2007). The analysis was performed with the following settings: seqtype = 1, CodonFreq = 2, Runmode = -2, and the transition/transversion ratio estimated from the data. To ensure reliability, genes exhibiting signs of saturated divergence or underestimated dS values were excluded, as codeml produces robust results only within a moderate range of sequence divergence. Specifically, we removed 43 orthologs with dN/dS $\geqq$ 99 and 483 genes with dS > 10, dS < 0.001, or dN < 0.0003. The thresholds of dN and dS were determined by examining the relationship between dN and dS and excluding outliers that deviated from the main distribution. After filtering, the final dataset comprised 11223 orthologous genes.

Linear regression analyses were performed to examine the relationship between dN, dS, dN/dS and peak month differences ($\Delta\varphi$) in gene expression between *Q. glauca* and *L. edulis*, as well as mean expression levels. These analyses were conducted using the lm function in R software (v 4.3.1). Specifically, we modeled the evolutionary rates (dN, dS, and dN/dS) as the response variable and the peak month difference ($\Delta\varphi$) or the mean levels in gene expression as the predictor variable. To account for the skewed distributions of evolutionary rates, logarithm transformations with base 2 were applied.

Data deposition and code availability

All sequencing data generated in this study have been deposited in the DNA Data Bank of Japan (DDBJ) and are available under the BioProject accession number PRJDB20498. RNA-seq reads used for expression analyses are available under the DDBJ Sequence Read Archive (DRA) run accession numbers DRR659185-DRR659374 and DRR664882-DRR665873, while DNA sequences used for genome assembly, genome size estimation and phylogenetic reconstruction are available under DRR659899-DRR659929. The assembled genomes are also available from DDBJ: the *Q. glauca* genome under accession numbers BAAHOF010000001-BAAHOF010000797, and the *L. edulis* genome under BAAHOE010000001-BAAHOE010000750. All codes used in the analysis are available at https://github.com/ku-biomath/Evolution_of_gene_expression_in_seasonal_envrionment.

Acknowledgments

We thank Atsuko Miyawaki-Kuwakado for her valuable technical advice on RNA-seq analysis. We also appreciate the technical support provided by Kayoko Ohta. Additionally, we thank Koharu Yamaguchi, Yuta Aoyagi, and Ryosuke Imai for their help with sample collection.

Additional information

Funding

This work was supported by JSPS KAKENHI Grant Numbers JP23H04965 and JP23H04966.

Author Contributions

S.N.K. and A.S. designed research; S.N.K., Y.I., J.K., H.H., S.I., and A.S. performed research; S.N.K., Y.I., J.K., H.H., S.I., and A.S. analyzed data; S.N.K. and A.S. wrote the paper with inputs from all the authors.

Competing Interest Statement

The authors declare no conflict of interest.

References

Aikawa S, Kobayashi MJ, Satake A, Shimizu KK, Kudoh H. 2010. Robust control of the seasonal expression of the Arabidopsis FLC gene in a fluctuating environment. *PNAS* **107**:11632–11637. doi:10.1073/pnas.0914293107

Bateman A, Martin M-J, Orchard S, Magrane M, Adesina A, Ahmad S, Bowler-Barnett EH, Bye-A-Jee H, Carpentier D, Denny P, Fan J, Garmiri P, Gonzales LJ da C, Hussein A, Ignatchenko A, Insana G, Ishtiaq R, Joshi V, Jyothi D, Kandasaamy S, Lock A, Luciani A, Luo J, Lussi Y, Marin JSM, Raposo P, Rice DL, Santos R, Speretta E, Stephenson J, Totoo P, Tyagi N, Urakova N, Vasudev P, Warner K, Wijerathne S, Yu CW-H, Zaru R, Bridge AJ, Aimo L, Argoud-Puy G, Auchincloss AH, Axelsen KB, Bansal P, Baratin D, Batista Neto TM, Blatter M-C, Bolleman JT, Boutet E, Breuza L, Gil BC, Casals-Casas

C, Echioukh KC, Coudert E, Cuche B, de Castro E, Estreicher A, Famiglietti ML, Feuermann M, Gasteiger E, Gaudet P, Gehant S, Gerritsen V, Gos A, Gruaz N, Hulo C, Hyka-Nouspikel N, Jungo F, Kerhornou A, Mercier P Le, Lieberherr D, Masson P, Morgat A, Paesano S, Pedruzzi I, Pilbout S, Pourcel L, Poux S, Pozzato M, Pruess M, Redaschi N, Rivoire C, Sigrist CJA, Sonesson K, Sundaram S, Sveshnikova A, Wu CH, Arighi CN, Chen C, Chen Y, Huang H, Laiho K, Lehvaslaiho M, McGarvey P, Natale DA, Ross K, Vinayaka CR, Wang Y, Zhang J. 2025. UniProt: the Universal Protein Knowledgebase in 2025. *Nucleic Acids Research* **53**:D609–D617. doi:10.1093/nar/gkae1010

Brawand D, Soumillon M, Necsulea A, Julien P, Csárdi G, Harrigan P, Weier M, Liechti A, Aximu-Petri A, Kircher M, Albert FW, Zeller U, Khaitovich P, Grützner F, Bergmann S, Nielsen R, Pääbo S, Kaessmann H. 2011. The evolution of gene expression levels in mammalian organs. *Nature* **478**:343–348. doi:10.1038/nature10532

Brůna T, Hoff KJ, Lomsadze A, Stanke M, Borodovsky M. 2021. BRAKER2: Automatic eukaryotic genome annotation with GeneMark-EP+ and AUGUSTUS supported by a protein database. *NAR Genomics and Bioinformatics* **3**:1–11. doi:10.1093/nargab/lqaa108

Buchfink B, Xie C, Huson DH. 2014. Fast and sensitive protein alignment using DIAMOND. *Nature Methods*. doi:10.1038/nmeth.3176

Camacho C, Coulouris G, Avagyan V, Ma N, Papadopoulos J, Bealer K, Madden TL. 2009. BLAST+: Architecture and applications. *BMC Bioinformatics* **10**. doi:10.1186/1471-2105-10-421

Cantalapiedra CP, Hernández-Plaza A, Letunic I, Bork P, Huerta-Cepas J. 2021. eggNOG-mapper v2: functional annotation, orthology assignments, and domain prediction at the metagenomic scale. *Molecular Biology and Evolution* **38**:5825–5829. doi:10.1093/molbev/msab293

Cardoso-Moreira M, Halbert J, Valloton D, Velten B, Chen C, Shao Y, Liechti A, Ascenção K, Rummel C, Ovchinnikova S, Mazin P V., Xenarios I, Harshman K, Mort M, Cooper DN, Sandi C, Soares MJ, Ferreira PG, Afonso S, Carneiro M, Turner JMA, VandeBerg JL, Fallahshahroudi A, Jensen P, Behr R, Lisgo S, Lindsay S, Khaitovich P, Huber W, Baker J, Anders S, Zhang YE, Kaessmann H. 2019. Gene expression across mammalian organ development. *Nature* **571**:505–509. doi:10.1038/s41586-019-1338-5

Chen LT, Wu K. 2010. Role of histone deacetylases HDA6 and HDA19 in ABA and abiotic stress response. *Plant Signaling & Behavior* **5**:1318–1320. doi:10.4161/psb.5.10.13168

861 Chen S, Zhou Y, Chen Y, Gu J. 2018. fastp: an ultra-fast all-in-one FASTQ
862 preprocessor. *Bioinformatics* **34**:i884–i890. doi:10.1093/bioinformatics/bty560

863 Chen SC, Cannon CH, Kua CS, Liu JJ, Galbraith DW. 2014. Genome size variation
864 in the Fagaceae and its implications for trees. *Tree Genetics and Genomes*
865 **10**:977–988. doi:10.1007/s11295-014-0736-y

866 Chikhi R, Medvedev P. 2014. Informed and automated k-mer size selection for
867 genome assembly. *Bioinformatics* **30**:31–37.
868 doi:10.1093/bioinformatics/btt310

869 Cleland EE, Wolkovich EM. 2024. Effects of phenology on plant community
870 assembly and structure. *Annual Review of Ecology, Evolution, and*
871 *Systematics* **55**:471–492. doi:10.1146/annurev-ecolsys-102722-011653

872 Dobin A, Davis CA, Schlesinger F, Drenkow J, Zaleski C, Jha S, Batut P, Chaisson
873 M, Gingeras TR. 2013. STAR: Ultrafast universal RNA-seq aligner.
874 *Bioinformatics* **29**:15–21. doi:10.1093/bioinformatics/bts635

875 Drost HG, Bellstädt J, Ó'Maoiléidigh DS, Silva AT, Gabel A, Weinholdt C, Ryan
876 PT, Dekkers BJW, Bentsink L, Hilhorst HWM, Ligterink W, Wellmer F, Grosse
877 I, Quint M. 2016. Post-embryonic hourglass patterns mark ontogenetic
878 transitions in plant development. *Mol Biol Evol* **33**:1158–1163.
879 doi:10.1093/molbev/msw039

880 Drummond DA, Bloom JD, Adami C, Wilke CO, Arnold FH. 2005. Why highly
881 expressed proteins evolve slowly. *PNAS* **102**:14338–14343.
882 doi:10.1073/pnas.0504070102

883 El Taher A, Böhne A, Boileau N, Ronco F, Indermaur A, Widmer L, Salzburger W.
884 2021. Gene expression dynamics during rapid organismal diversification in
885 African cichlid fishes. *Nature Ecology and Evolution* **5**:243–250.
886 doi:10.1038/s41559-020-01354-3

887 Emanuelle S, Doblin MS, Stapleton DI, Bacic A, Gooley PR. 2016. Molecular
888 insights into the enigmatic metabolic regulator, SnRK1. *Trends in Plant*
889 *Science* **21**:341–353. doi:10.1016/j.tplants.2015.11.001

890 Emms DM, Kelly S. 2019. OrthoFinder: Phylogenetic orthology inference for
891 comparative genomics. *Genome Biology* **20**. doi:10.1186/s13059-019-1832-y

892 Falcon S, Gentleman R. 2007. Using GOstats to test gene lists for GO term
893 association. *Bioinformatics* **23**:257–258. doi:10.1093/bioinformatics/btl567

894 Fan H, Ives AR, Surget-Groba Y, Cannon CH. 2015. An assembly and alignment-
895 free method of phylogeny reconstruction from next-generation sequencing
896 data. *BMC Genomics* **16**. doi:10.1186/s12864-015-1647-5

Fischl H, McManus D, Oldenkamp R, Schermelleh L, Mellor J, Jagannath A, Furger A. 2020. Cold-induced chromatin compaction and nuclear retention of clock mRNAs resets the circadian rhythm. *EMBO Journal* **39**. doi:10.15252/embj.2020105604

Forrest J, Miller-Rushing AJ. 2010. Toward a synthetic understanding of the role of phenology in ecology and evolution. *Philosophical Transactions of the Royal Society B: Biological Sciences* **365**:3101–3112. doi:10.1098/rstb.2010.0145

Fretwell SD. 1972. Populations in a seasonal environment. *Monographs in Population Biology* **5**:1–217.

Gaut B, Yang L, Takuno S, Eguiarte LE. 2011. The patterns and causes of variation in plant nucleotide substitution rates. *Annual Review of Ecology, Evolution, and Systematics* **42**:245–266. doi:10.1146/annurev-ecolsys-102710-145119

Hernández-Plaza A, Szklarczyk D, Botas J, Cantalapiedra CP, Giner-Lamia J, Mende DR, Kirsch R, Rattei T, Letunic I, Jensen LJ, Bork P, von Mering C, Huerta-Cepas J. 2023. eggNOG 6.0: enabling comparative genomics across 12 535 organisms. *Nucleic Acids Research* **51**:D389–D394. doi:10.1093/nar/gkac1022

Hipp AL, Manos PS, Hahn M, Avishai M, Bodénès C, Cavender-Bares J, Crowl AA, Deng M, Denk T, Fitz-Gibbon S, Gailing O, González-Elizondo MS, González-Rodríguez A, Grimm GW, Jiang XL, Kremer A, Lesur I, McVay JD, Plomion C, Rodríguez-Correa H, Schulze ED, Simeone MC, Sork VL, Valencia-Avalos S. 2020. Genomic landscape of the global oak phylogeny. *New Phytologist* **226**:1198–1212. doi:10.1111/nph.16162

Ikezaki Y, Kudo SN, Nakata T, Koita S, Munakata R, Yazaki K, Torimaru T, Tomaru N, Isobe S, Hirakawa H, Kusumi J, Satake A. 2025. Molecular evolution of terpene synthase underlying the diversification of isoprene emission in Fagaceae. doi:10.1101/2025.07.31.667835

Irie N, Kuratani S. 2011. Comparative transcriptome analysis reveals vertebrate phylotypic period during organogenesis. *Nature Communications* **2**. doi:10.1038/ncomms1248

Kalinka AT, Varga KM, Gerrard DT, Preibisch S, Corcoran DL, Jarrells J, Ohler U, Bergman CM, Tomancak P. 2010. Gene expression divergence recapitulates the developmental hourglass model. *Nature* **468**:811–816. doi:10.1038/nature09634

Kant P, Kant S, Gordon M, Shaked R, Barak S. 2007. Stress Response Suppressor1 and Stress Response Suppressor2, two Dead-box RNA helicases that attenuate Arabidopsis responses to multiple abiotic stresses. *Plant Physiology* **145**:814–830. doi:10.1104/pp.107.099895

936 Keilwagen J, Hartung F, Grau J. 2019. GeMoMa: Homology-based gene prediction
937 utilizing intron position conservation and RNA-seq data *Methods in Molecular*
938 *Biology*. Humana Press Inc. pp. 161–177. doi:10.1007/978-1-4939-9173-0_9

939 Kim D, Paggi JM, Park C, Bennett C, Salzberg SL. 2019. Graph-based genome
940 alignment and genotyping with HISAT2 and HISAT-genotype. *Nature*
941 *Biotechnology* **37**:907–915. doi:10.1038/s41587-019-0201-4

942 Kokot M, Dlugosz M, Deorowicz S. 2017. KMC 3: counting and manipulating k-mer
943 statistics. *Bioinformatics* **33**:2759–2761. doi:10.1093/bioinformatics/btx304

944 Komoto H, Nagahama A, Miyawaki-Kuwakado A, Hata Y, Kyozuka J, Kajita Y,
945 Toyama H, Satake A. 2024. The transcriptional changes underlying the
946 flowering phenology shift of *Arabidopsis halleri* in response to climate warming.
947 *Plant Cell & Environment* **47**:174–186. doi:10.1111/pce.14716

948 Kremer A, Abbott AG, Carlson JE, Manos PS, Plomion C, Sisco P, Staton ME,
949 Ueno S, Vendramin GG. 2012. Genomics of Fagaceae. *Tree Genetics &*
950 *Genomes* **8**:583–610. doi:10.1007/s11295-012-0498-3

951 Krishnakumar V, Hanlon MR, Contrino S, Ferlanti ES, Karamycheva S, Kim M,
952 Rosen BD, Cheng CY, Moreira W, Mock SA, Stubbs J, Sullivan JM, Krampis
953 K, Miller JR, Micklem G, Vaughn M, Town CD. 2015. Araport: The Arabidopsis
954 Information Portal. *Nucleic Acids Research* **43**:D1003–D1009.
955 doi:10.1093/nar/gku1200

956 Kubo T, Iwasa Y. 1996. Phenological pattern of tree regeneration in a model for
957 forest species diversity. *Theoretical Population Biology* **49**:90–117.
958 doi:10.1006/tpbi.1996.0004

959 Kudoh H. 2016. Molecular phenology in plants: *in natura* systems biology for the
960 comprehensive understanding of seasonal responses under natural
961 environments. *New Phytologist* **210**:399–412. doi:10.1111/nph.13733

962 Lemos B, Bettencourt BR, Meiklejohn CD, Hartl DL. 2005. Evolution of proteins
963 and gene expression levels are coupled in *Drosophila* and are independently
964 associated with mRNA abundance, protein length, and number of protein-
965 protein interactions. *Molecular Biology and Evolution* **22**:1345–1354.
966 doi:10.1093/molbev/msi122

967 Levin M, Anavy L, Cole AG, Winter E, Mostov N, Khair S, Senderovich N, Kovalev
968 E, Silver DH, Feder M, Fernandez-Valverde SL, Nakanishi N, Simmons D,
969 Simakov O, Larsson T, Liu SY, Jerafi-Vider A, Yaniv K, Ryan JF, Martindale
970 MQ, Rink JC, Arendt D, Degnan SM, Degnan BM, Hashimshony T, Yanai I.
971 2016. The mid-developmental transition and the evolution of animal body
972 plans. *Nature* **531**:637–641. doi:10.1038/nature16994

973 Li B, Dewey CN. 2011. RSEM: Accurate transcript quantification from RNA-Seq
974 data with or without a reference genome. *BMC Bioinformatics* **12**.
975 doi:10.1186/1471-2105-12-323

976 Li H, Durbin R. 2009. Fast and accurate short read alignment with Burrows-
977 Wheeler transform. *Bioinformatics* **25**:1754–1760.
978 doi:10.1093/bioinformatics/btp324

979 Liao BY, Zhang J. 2006. Low rates of expression profile divergence in highly
980 expressed genes and tissue-specific genes during mammalian evolution.
981 *Molecular Biology and Evolution* **23**:1119–1128. doi:10.1093/molbev/msj119

982 Liu H, Zhang R, Zhou BF, Shen Z, Chen XY, Gao J, Wang B. 2023. Chromosome-
983 scale genome assembly of sweet tea (Lithocarpus polystachyus Rehder).
984 *Scientific Data* **10**. doi:10.1038/s41597-023-02791-y

985 Lotharukpong JS, Zheng M, Luthringer R, Liesner D, Drost H-G, Coelho SM. 2024.
986 A transcriptomic hourglass in brown algae. *Nature* **635**:129–135.
987 doi:10.1038/s41586-024-08059-8

988 Manos PS, Zhou Z, Cannon CH. 2001. Systematics of Fagaceae: phylogenetic
989 tests of reproductive trait evolution. *International Journal of Plant Sciences*
990 **162**:1361–1379. doi:10.1086/322949

991 Mishra B, Ulaszewski B, Meger J, Aury JM, Bodénès C, Lesur-Kupin I, Pfenninger
992 M, Da Silva C, Gupta DK, Guichoux E, Heer K, Lalanne C, Labadie K,
993 Opgenoorth L, Ploch S, Le Provost G, Salse J, Scotti I, Wötzel S, Plomion C,
994 Burczyk J, Thines M. 2022. A chromosome-level genome assembly of the
995 European Beech (Fagus sylvatica) reveals anomalies for organelle DNA
996 integration, repeat content and distribution of SNPs. *Frontiers in Genetics* **12**.
997 doi:10.3389/fgene.2021.691058

998 Miyawaki‐Kuwakado A, Han Q, Kitamura K, Satake A. 2024. Impacts of climate
999 change on the transcriptional dynamics and timing of bud dormancy release
1000 in Yoshino‐cherry tree. *PLANTS, PEOPLE, PLANET* **6**:1505–1521.
1001 doi:10.1002/ppp3.10548

1002 Miyazaki Y, Maruyama Y, Chiba Y, Kobayashi MJ, Joseph B, Shimizu KK, Mochida
1003 K, Hiura T, Kon H, Satake A. 2014. Nitrogen as a key regulator of flowering in
1004 Fagus crenata: Understanding the physiological mechanism of masting by
1005 gene expression analysis. *Ecology Letters* **17**:1299–1309.
1006 doi:10.1111/ele.12338

1007 Morellato LPC, Camargo MGG, Gressler E. 2013. "A review of plant phenology in
1008 South and Central America." in Phenology: An Integrative Environmental
1009 Science. Springer.

1010 Nagano AJ, Kawagoe T, Sugisaka J, Honjo MN, Iwayama K, Kudoh H. 2019.
1011 Annual transcriptome dynamics in natural environments reveals plant
1012 seasonal adaptation. *Nature Plants* **5**:74–83. doi:10.1038/s41477-018-0338-
1013 z

1014 Naqvi S, Godfrey AK, Hughes JF, Goodheart ML, Mitchell RN, Page DC. 2019.
1015 Conservation, acquisition, and functional impact of sex-biased gene
1016 expression in mammals. *Science (1979)* **365**. doi:10.1126/science.aaw7317

1017 Nishio H, Nagano AJ, Ito T, Suzuki Y, Kudoh H. 2020. Seasonal plasticity and diel
1018 stability of H3K27me3 in natural fluctuating environments. *Nature Plants*
1019 **6**:1091–1097. doi:10.1038/s41477-020-00757-1

1020 Nuzhdin S V., Wayne ML, Harmon KL, McIntyre LM. 2004. Common pattern of
1021 evolution of gene expression level and protein sequence in Drosophila.
1022 *Molecular Biology and Evolution* **21**:1308–1317. doi:10.1093/molbev/msh128

1023 Patro R, Duggal G, Love MI, Irizarry RA, Kingsford C. 2017. Salmon provides fast
1024 and bias-aware quantification of transcript expression. *Nature Methods*
1025 **14**:417–419. doi:10.1038/nmeth.4197

1026 Pertea M, Pertea G. 2020. GFF Utilities: GffRead and GffCompare. *F1000Res* **9**.
1027 doi:10.12688/f1000research.23297.1

1028 Piao S, Liu Q, Chen A, Janssens IA, Fu Y, Dai J, Liu L, Lian X, Shen M, Zhu X.
1029 2019. Plant phenology and global climate change: Current progresses and
1030 challenges. *Global Change Biology* **25**:1922–1940. doi:10.1111/gcb.14619

1031 Prud'homme B, Gompel N, Carroll SB. 2007. Emerging principles of regulatory
1032 evolution. *PNAS* **104**:8605–8612. doi:10.1073/pnas.0700488104

1033 Putnam NH, O'Connell BL, Stites JC, Rice BJ, Blanchette M, Calef R, Troll CJ,
1034 Fields A, Hartley PD, Sugnet CW, Haussler D, Rokhsar DS, Green RE. 2016.
1035 Chromosome-scale shotgun assembly using an in vitro method for long-range
1036 linkage. *Genome Research* **26**:342–350. doi:10.1101/gr.193474.115

1037 Quint M, Drost HG, Gabel A, Ullrich KK, Bönn M, Grosse I. 2012. A transcriptomic
1038 hourglass in plant embryogenesis. *Nature* **490**:98–101.
1039 doi:10.1038/nature11394

1040 Ranallo-Benavidez TR, Jaron KS, Schatz MC. 2020. GenomeScope 2.0 and
1041 Smudgeplot for reference-free profiling of polyploid genomes. *Nature*
1042 *Communications* **11**. doi:10.1038/s41467-020-14998-3

1043 Satake A, Hagiwara T, Nagano AJ, Yamaguchi N, Sekimoto K, Shiojiri K, Sudo K.
1044 2024a. Plant molecular phenology and climate feedbacks mediated by
1045 BVOCs. *Annual Review of Plant Biology* **75**:605–627. doi:10.1146/annurev-
1046 arplant-060223-032108

1047 Satake A, Imai R, Fujino T, Tomimoto S, Ohta K, Na'iem M, Indrioko S, Widiyatno
1048 W, Purnomo S, Morales AM, Nizhynska V, Tani N, Suyama Y, Sasaki E,
1049 Kasahara M. 2024b. Somatic mutation rates scale with time not growth rate in
1050 long-lived tropical trees. *Elife* **12**. doi:10.7554/eLife.88456

1051 Satake A, Nagahama A, Sasaki E. 2022. A cross‐scale approach to unravel the
1052 molecular basis of plant phenology in temperate and tropical climates. *New*
1053 *Phytologist* **233**:2340–2353. doi:10.1111/nph.17897

1054 Satake A, Ohta K, Takeda-Kamiya N, Toyooka K, Kusumi J. 2023. Seasonal gene
1055 expression signatures of delayed fertilization in Fagaceae. *Molecular Ecology*
1056 **32**:4801–4813. doi:10.1111/mec.17079

1057 Schwartz MD. 2013. Phenology: An Integrative Environmental Science, 2nd ed.
1058 Springer Dordrecht.

1059 Smaczniak C, Immink RGH, Muiño JM, Blanvillain R, Busscher M, Busscher-
1060 Lange J, Dinh QD, Liu S, Westphal AH, Boeren S, Parcy F, Xu L, Carles CC,
1061 Angenent GC, Kaufmann K. 2012. Characterization of MADS-domain
1062 transcription factor complexes in *Arabidopsis* flower development. *PNAS*
1063 **109**:1560–1565. doi:10.1073/pnas.1112871109

1064 Smid M, Coebergh van den Braak RRJ, van de Werken HJG, van Riet J, van Galen
1065 A, de Weerd V, van der Vlugt-Daane M, Bril SI, Lalmahomed ZS, Kloosterman
1066 WP, Wilting SM, Foekens JA, IJzermans JNM, Martens JWM, Sieuwerts AM.
1067 2018. Gene length corrected trimmed mean of M-values (GeTMM) processing
1068 of RNA-seq data performs similarly in intersample analyses while improving
1069 intrasample comparisons. *BMC Bioinformatics* **19**. doi:10.1186/s12859-018-
1070 2246-7

1071 Thaben PF, Westermark PO. 2014. Detecting rhythms in time series with rain.
1072 *Journal of Biological Rhythms* **29**:391–400. doi:10.1177/0748730414553029

1073 True JR, Haag ES. 2001. Developmental system drift and flexibility in evolutionary
1074 trajectories. *Evolution & Development* **3**:109–119. doi:10.1046/j.1525-
1075 142x.2001.003002109.x

1076 Wang Y, Tang H, Debarry JD, Tan X, Li J, Wang X, Lee TH, Jin H, Marler B, Guo
1077 H, Kissinger JC, Paterson AH. 2012. MCScanX: A toolkit for detection and
1078 evolutionary analysis of gene synteny and collinearity. *Nucleic Acids*
1079 *Research* **40**. doi:10.1093/nar/gkr1293

1080 Yang L, Gaut BS. 2011. Factors that contribute to variation in evolutionary rate
1081 among arabidopsis genes. *Molecular Biology and Evolution* **28**:2359–2369.
1082 doi:10.1093/molbev/msr058

1083 Yang Z. 2007. PAML 4: Phylogenetic analysis by maximum likelihood. *Molecular*
1084 *Biology and Evolution* **24**:1586–1591. doi:10.1093/molbev/msm088

1085 Yoo SJ, Chung KS, Jung SH, Yoo SY, Lee JS, Ahn JH. 2010. BROTHER of FT
1086 and TFL1 (BFT) has TFL1-like activity and functions redundantly with TFL1 in
1087 inflorescence meristem development in *Arabidopsis*. *Plant Journal* **63**:241–
1088 253. doi:10.1111/j.1365-313X.2010.04234.x

1089 Zhang X, Yu G, Dai Y, Zhang H, Wang K, Han J. 2023. High-resolution Hi-C maps
1090 highlight multiscale chromatin architecture reorganization during cold stress in
1091 Brachypodium distachyon. *BMC Plant Biology* **23**. doi:10.1186/s12870-023-
1092 04269-w

1093 Zhou BF, Yuan S, Crowl AA, Liang YY, Shi Y, Chen XY, An QQ, Kang M, Manos
1094 PS, Wang B. 2022. Phylogenomic analyses highlight innovation and
1095 introgression in the continental radiations of Fagaceae across the Northern
1096 Hemisphere. *Nature Communications* **13**. doi:10.1038/s41467-022-28917-1

1097 Zhu GQ, Qu L, Xue HW. 2024. Casein kinase 1 AELs promote senescence by
1098 enhancing ethylene biosynthesis through phosphorylating WRKY22
1099 transcription factor. *New Phytologist* **244**:116–130. doi:10.1111/nph.19785

1100 Zoldos V, Papes D, Cerbah M, Panaud O, Besendorfer V, Siljak-Yakovlev S. 1999.
1101 Molecular-cytogenetic studies of ribosomal genes and heterochromatin reveal
1102 conserved genome organization among 11 Quercus species. *Theoretical and*
1103 *Applied Genetics* **99**:969–977. doi:10.1007/s001220051404

1104 Zrimec J, Börlin CS, Buric F, Muhammad AS, Chen R, Siewers V, Verendel V,
1105 Nielsen J, Töpel M, Zelezniak A. 2020. Deep learning suggests that gene
1106 expression is encoded in all parts of a co-evolving interacting gene regulatory
1107 structure. *Nature Communications* **11**. doi:10.1038/s41467-020-19921-4

1108 Zrimec J, Buric F, Kokina M, Garcia V, Zelezniak A. 2021. Learning the Regulatory
1109 Code of Gene Expression. *Frontiers in Molecular Biosciences* **8**.
1110 doi:10.3389/fmolb.2021.673363

1111
1112

1113 **Figures**

1114 **Figure 1.** Synteny and distribution of genomic features of *Q. glauca* and *L. edulis*
1115 genomes. (A) A phylogenetic tree of five Fagaceae species from three genera,
1116 *Quercus*, *Lithocarpus*, and *Fagus*. Bootstrap values for all branches are 100. (B)
1117 Synteny relationship between the *Q. glauca* and *L. edulis* genomes. The collinear
1118 blocks within the genomes were displayed by lines. Black lines show reverse
1119 alignment and gray lines represent regular. Numbers correspond to the 12
1120 chromosomes. (C–D) Circos plots of the *Q. glauca* (C) and *L. edulis* genomes (D).
1121 Lanes depict circular representation of chromosome length (Mbp) (a), gene density
1122 (b), GC density (c), and repeat (d). Lines in the inner circle represent links between
1123 synteny-selected paralogs. (E) Orthogroup classification based on the orthogroup
1124 size difference between the *Q. glauca* and *L. edulis* genomes. The bar plot
1125 illustrates the number of genes in gene families categorized into 1:1 orthologs, N:N
1126 (many-to-many), 1:N (one-to-many), N:1 (many-to-one), and species-specific
1127 unique genes. (F–G) Mean gene expression levels in each copy number variation

category for *Q. glauca* (F) and *L. edulis* (G). Different letters denote statistically significant differences ($p < 0.05$, Steel-Dwass test).

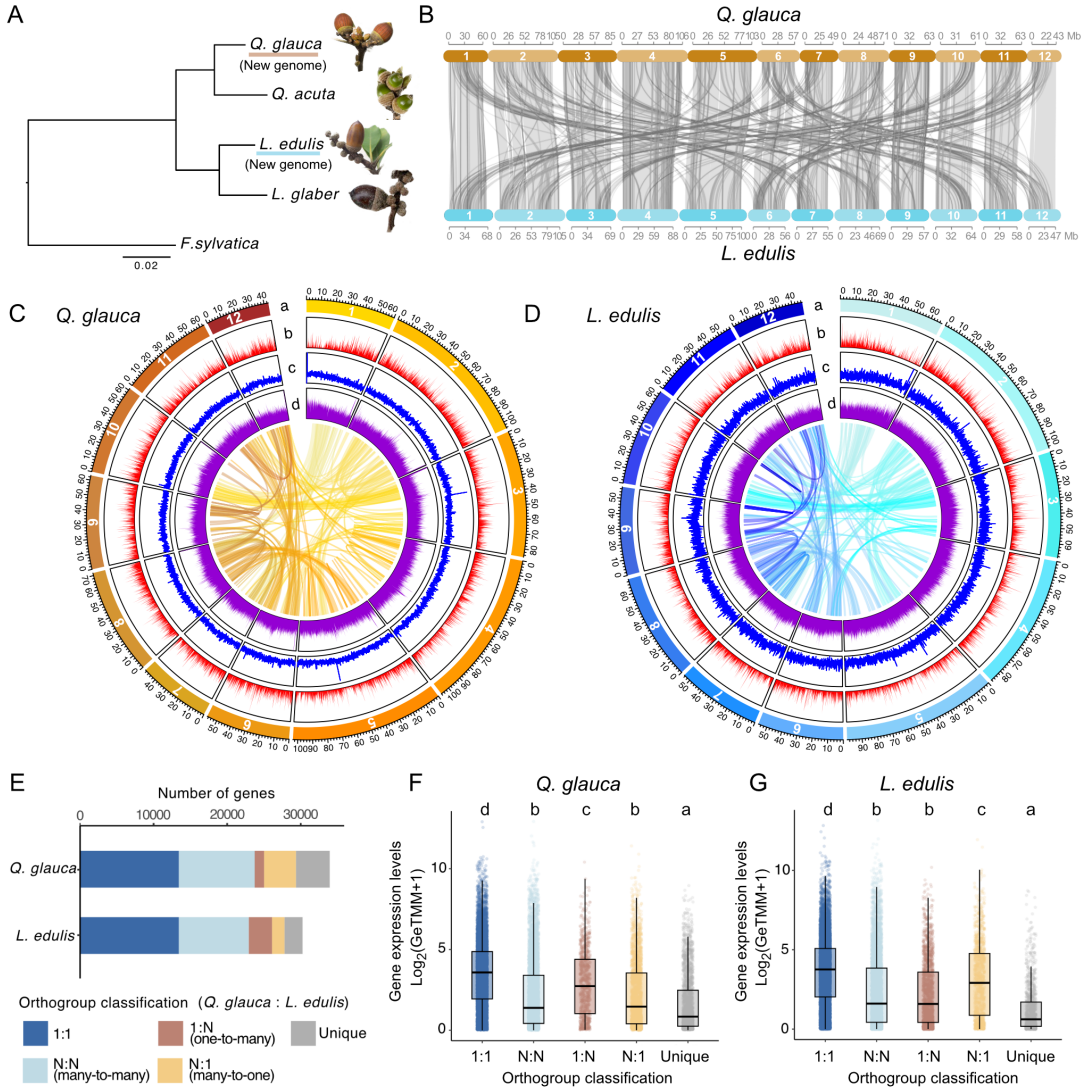

Figure 2. Seasonal gene expression dynamics. (A) Hierarchical clustering of 213 time points encompassing two tissues (leaf and bud) and four species (*Q. glauca*, *Q. acuta*, *L. edulis*, and *L. glaber*), collected over two-year. Newly flushed leaf samples are indicated as asterisks. (B) Distribution of daily mean temperature on each sampling date across clusters, from L1 (top) to B3 (bottom). The Mann-Whitney U test was used to compare daily mean temperature between cluster L1 and L2 (p = 0.136). The Steel-Dwass test was applied for multiple comparisons across clusters B1–B3 (p < 0.05). Different letters denote statistically significant differences (p < 0.05). (C–D) Hierarchical clustering of 11749 genes based on the similarity of gene expression dynamics. Daily mean temperature, flowering and leaf flushing phenology (proportion) are shown in the upper three panels of the heatmaps.

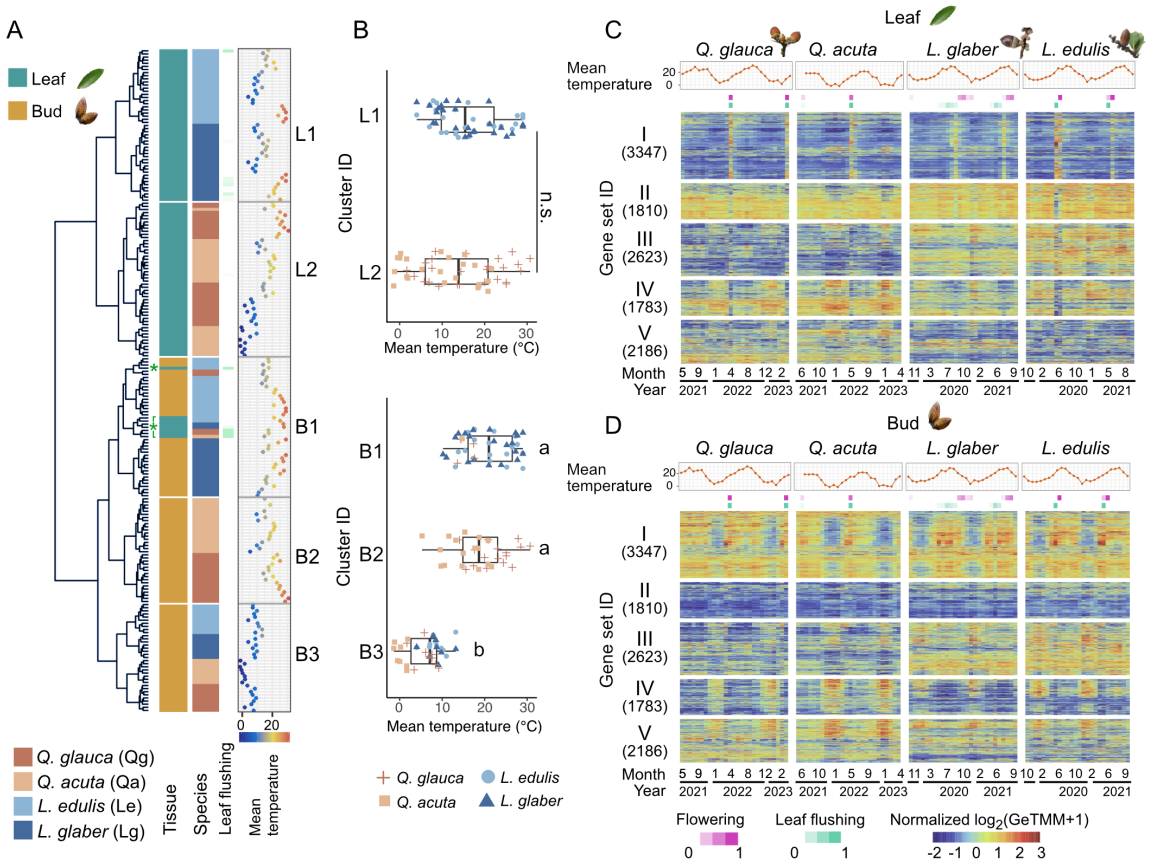

Figure 3. Distribution of period and peak month in rhythmic gene expression. (A–B) Distribution of period length (month) among the genes with significant rhythmicity calculated by RAIN for leaf (A) and bud (B) samples of each species. (C–D) Distribution of seasonal peaks among the genes with annual periodicity. The angle of each bar represents the peak month, while the bar height indicates the number of genes. Blue arrows indicate the month with the highest number of genes peaking during winter (December–February), while red arrows indicate the month with the highest number of genes peaking during the growing season (March–November). Purple and green squares around each rose plot denote the observed phenology of flowering and leaf flushing (proportion), respectively.

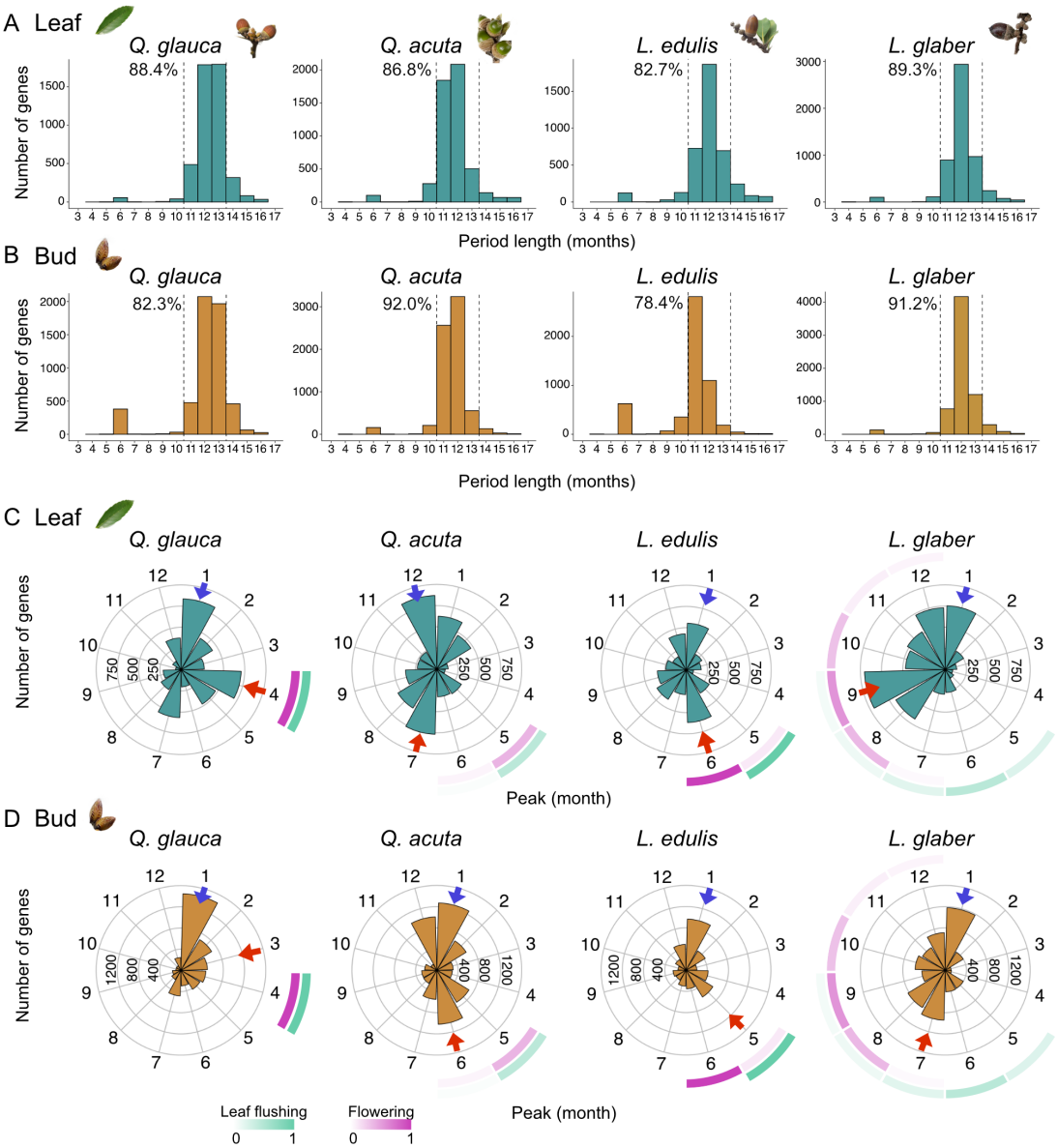

Figure 4. Comparison of peak months in seasonal gene expression across species in buds. (A) Intra-genus and (B) inter-genera comparisons of peak months in seasonal gene expression. The size and color of the circles represent the number of genes and the mean of Pearson's correlation, respectively. Genes with negative correlations lower than -0.3 are highlighted in blue, while the month of leaf flushing is highlighted in green. (C) Plot of molecular phenology divergence index *D* across months. Triangles and circles indicate the values of *D* calculated from intra-genus and inter-genera comparison, respectively. The line and shaded envelope indicate the mean and standard deviation (s.d.). Different letters denote statistically significant differences (Nemenyi test, $p < 0.05$).

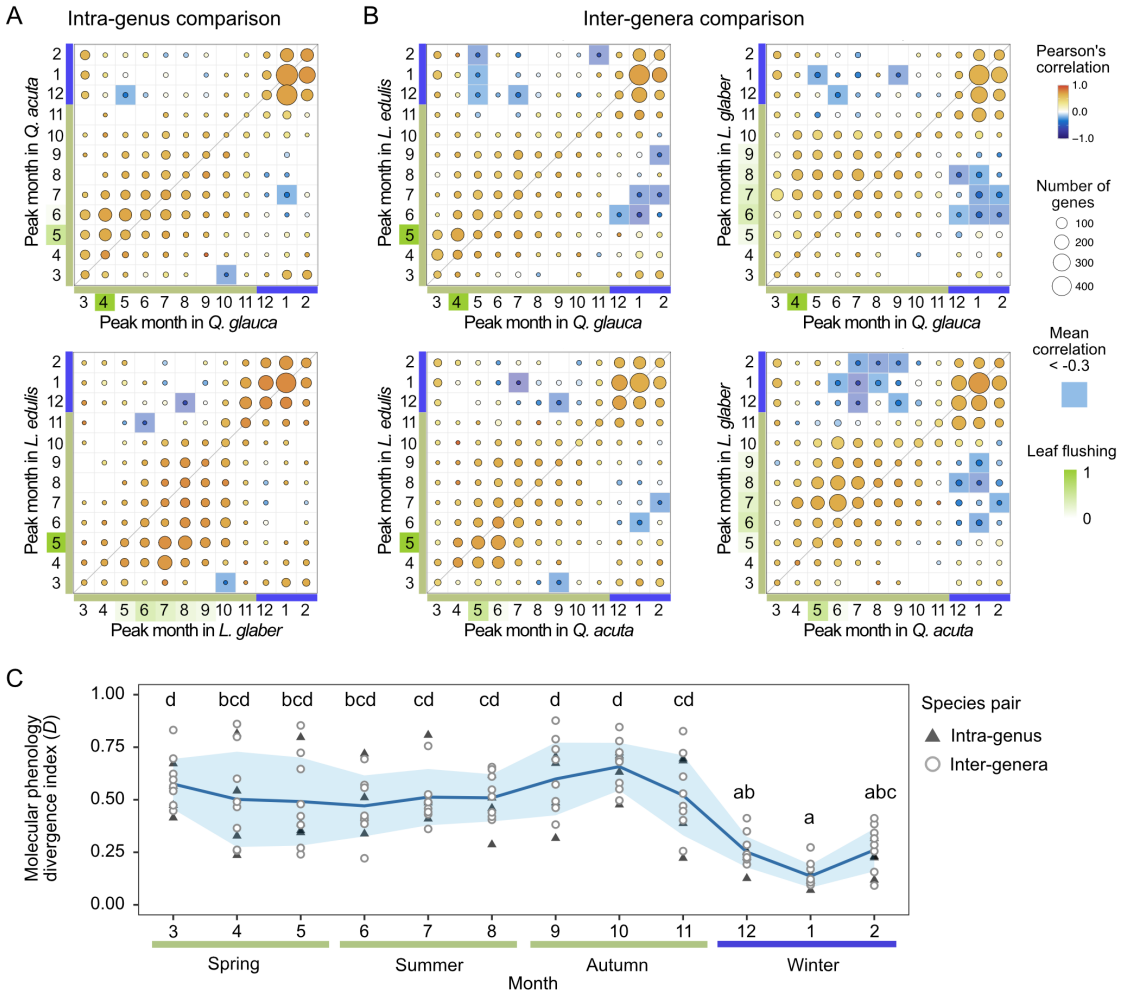

Figure 5. Phylogenetic constraints in the evolution of seasonal gene expression and the relationship between seasonal gene expression divergence and sequence evolution. (A) Distribution of pairwise Pearson's correlation coefficients for gene expression across species (Le: *L. edulis*, Lg: *L. glaber*, Qg: *Q. glauca*, Qa: *Q. acuta*; n = 11749). Colors indicate rhythmicity categories. Black bars show median correlation values, and different letters indicate significant differences (Nemenyi test, $p < 0.05$). (B) Heatmap of pairwise correlation coefficients for each gene, with mean gene counts in four seasonal expression categories: (1) annual rhythmic genes peaking in the growing season (March–November), (2) annual rhythmic genes peaking in winter (December–February), (3) half-annual rhythmic genes, and (4) arrhythmic genes. Genes are ordered by mean correlation across species pairs. (C–D) Conserved (C) and diverged (D) gene expression patterns, based on the top and bottom 5% of pairwise correlations. Solid lines and error bars indicate mean ± SD. Numbers in parentheses show peak month differences between *Q. glauca* and *L. edulis*. Peak month difference for *BFT* was not calculated due to arrhythmic expression in *Q. glauca*. (E) Relationship between evolutionary rate (dN/dS) and peak month difference ($\Delta\varphi$) for genes with annual periodicity in *Q. glauca* and *L. edulis* (n = 951). Black lines and transparent bands represent regression lines and 95% confidence intervals. The regression coefficient (β) and corresponding p-value are shown in each panel.

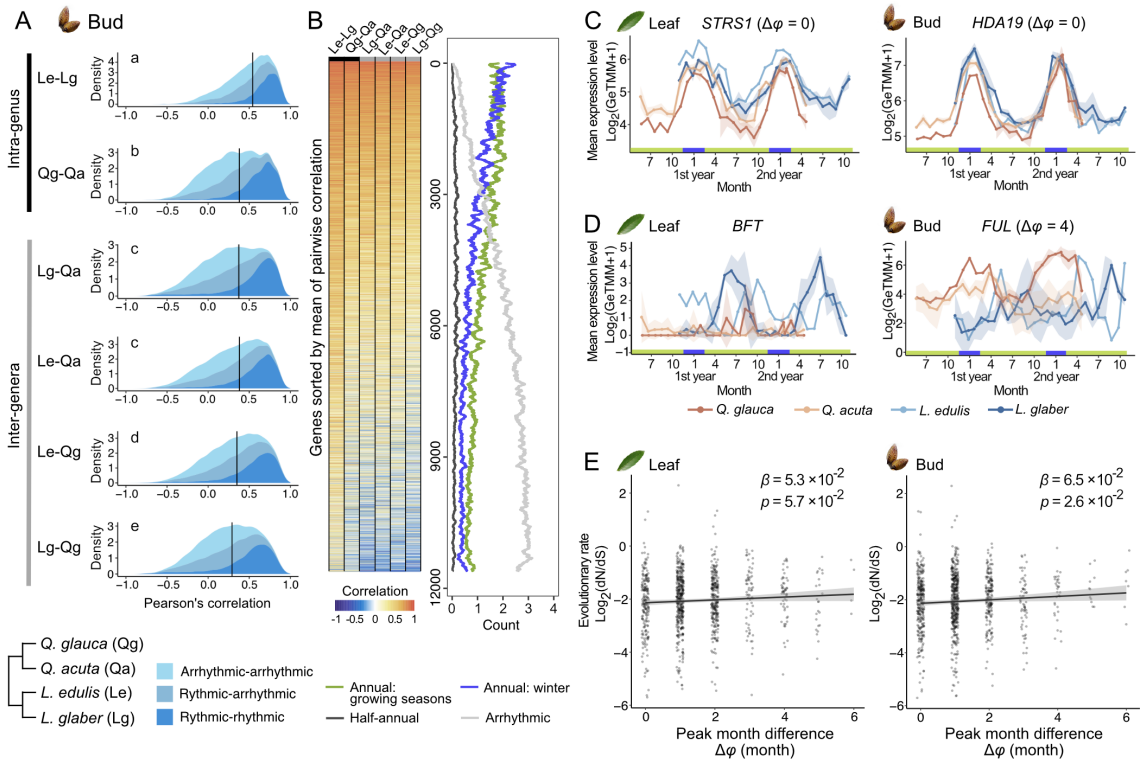

Supplementary figures

Figure S1. Dynamic range of gene expression in seasonal environments. (A) Dynamic range of seasonal gene expression in leaves and buds for *Q. glauca*, *Q. acuta*, *L. edulis*, and *L. glaber*. Each dot represents an expression level ($\log_2$(GeTMM+1)) on each sampling date, while black lines indicate the mean expression level of each gene over the entire sampling period. The bars on the left side of the panels distinguish between rhythmic (blue) and arhythmic (gray) genes. (B) Density plots showing the distribution of the ratio of standard deviation divided by the mean for each gene (σ_i / μ_i) and the overall variation across all genes in the genome (σ_g/μ_g) in leaves and buds for *Q. glauca, Q. acuta, L. edulis,* and *L. glaber*.

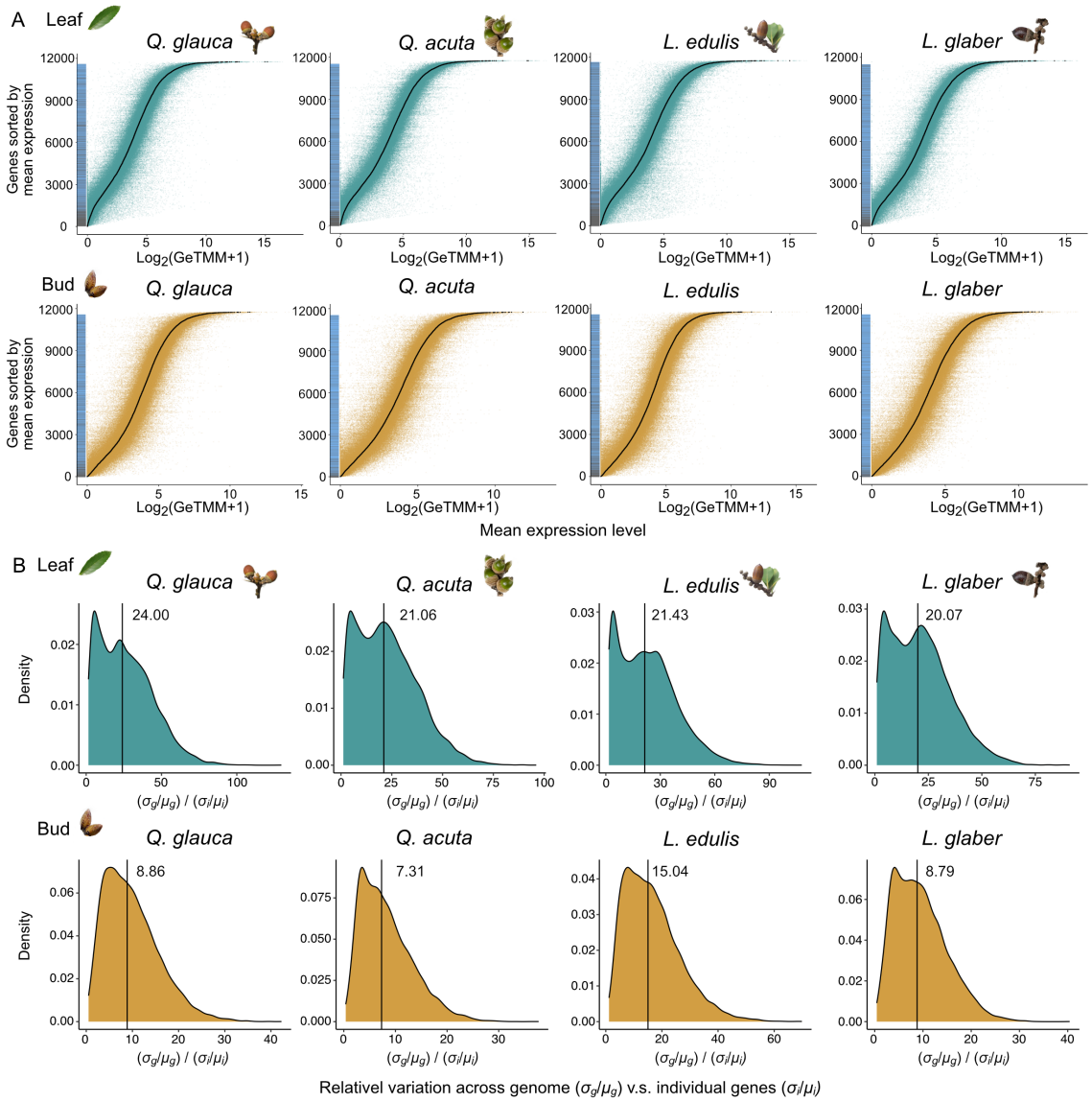

1206 **Figure S2.** Comparison of gene expression across individuals. Scatter plots
1207 showing the expression levels of each gene measured from different individuals
1208 for *L. glaber* (A), *Q. glauca* (B), and *Q. acuta* (C). The Pearson's correlation
1209 coefficient for each pair of individuals is shown in the corresponding panel.

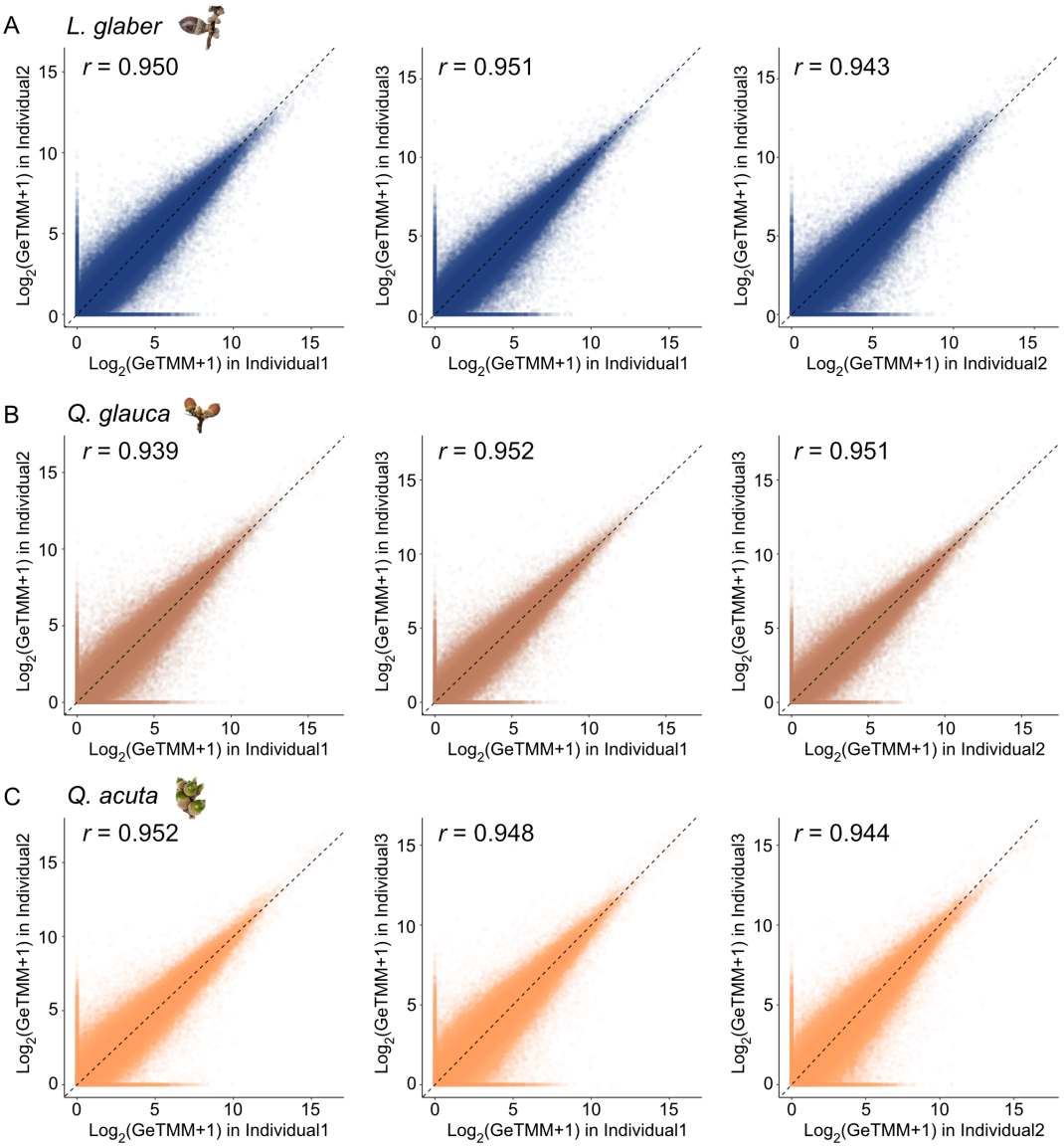

1210

1211

Figure S3. Seasonal fluctuations in environmental factors at the three study sites. Daily mean temperature and photoperiods at the three study sites (Ito campus, Kyushu university; Imajuku Field Activity Center; Mt. Sefuri in Kyushu, Japan) during the monitoring periods. The solid lines indicate the daily mean temperature, and the shaded area indicates the photoperiod. The study sites are located within a relatively small region, with distances between them ranging from approximately 10 to 20 km. The elevations vary, with Ito Campus (20–57 m a.s.l.) and Imajuku Field Activity Center (84–111 m a.s.l.) at lower altitudes, while Mt. Sefuri is at a higher elevation (970–974 m a.s.l.). Environmental data from Ito Campus and the Imajuku Field Activity Center were obtained from the Japan Meteorological Agency, while data from Sefuri Mountain were collected using a logger installed at the sampling site since July 15, 2021.

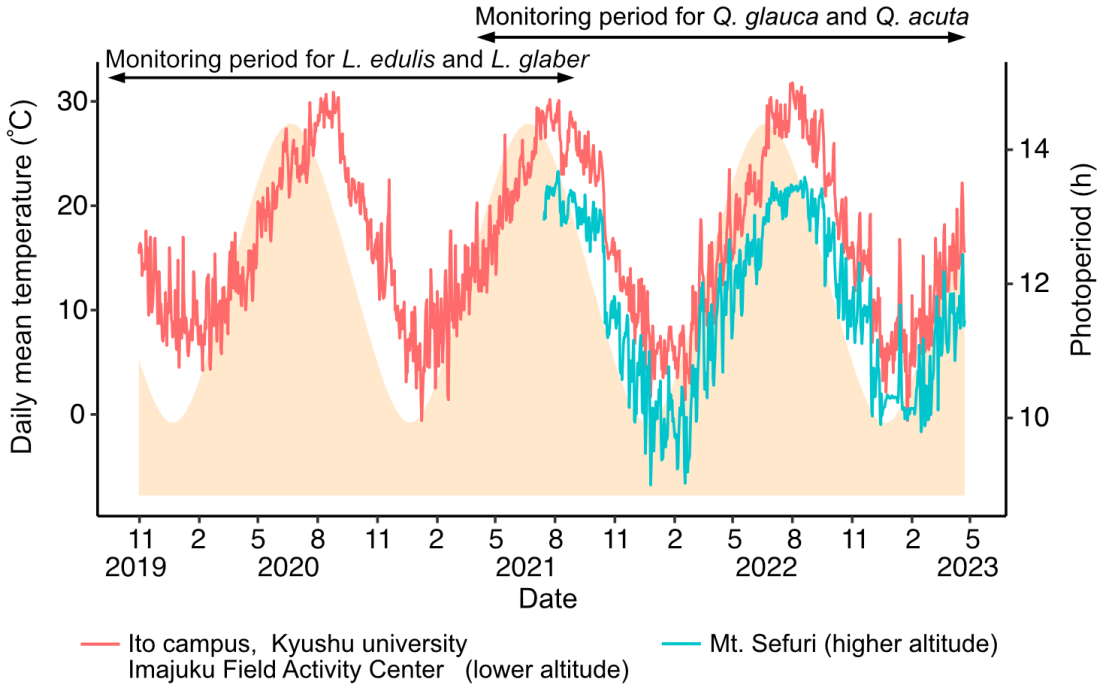

Figure S4. Determining the optimal number of clusters in hierarchical clustering. (A) Relationship between the number of clusters *k* and total Within-Cluster-Sum of Squared Error (WSS) on the clustering of 213 samples. We adopted the optimal *k* = 5 because it was the elbow point of the curve. (B) Relationship between the number of clusters *k* and total WSS on the clustering of 11749 genes. The elbow point was *k* = 4 or 5 and we selected the number of cluster *k* = 5. If *k* = 4 is selected, gene set IV and V (Fig. 2D, E in main text) are merged.

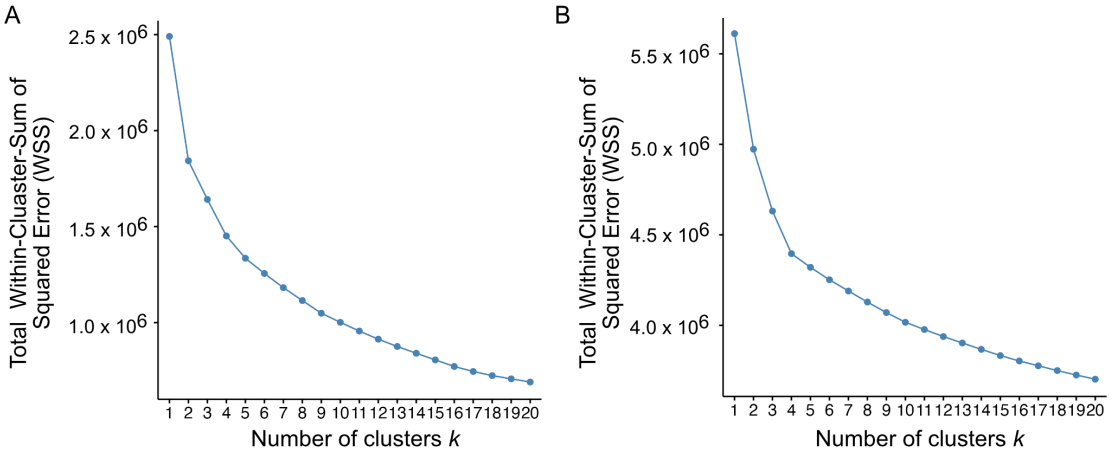

Figure S5. Phenological observations of leaf flushing, flowering (male and female flower) and winter buds of the four target species.

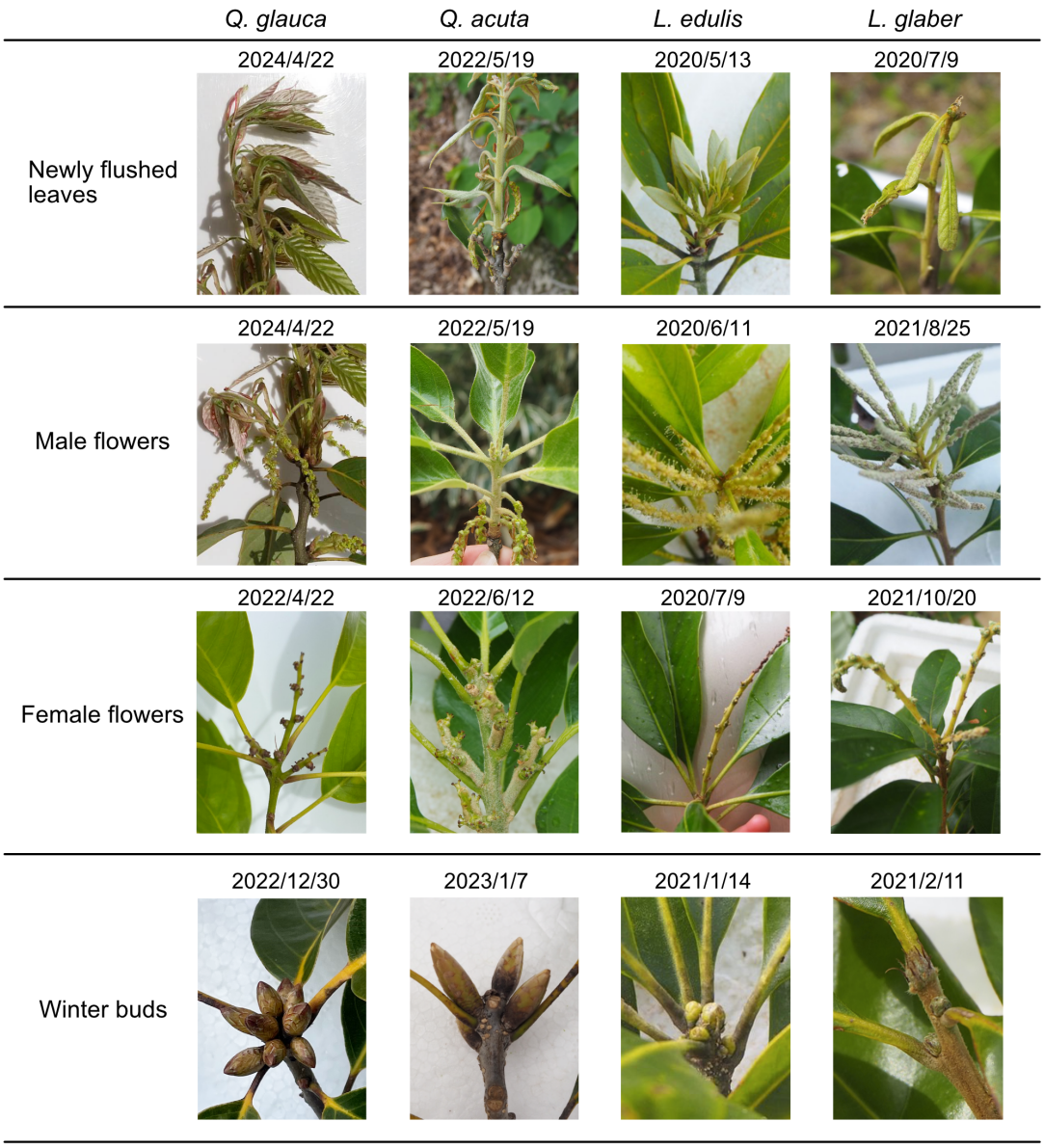

Figure S6. Seasonal gene expression dynamics observed within the same sampling period (from May 2021 to October 2022). (A) Hierarchical clustering of 160 time points encompassing two tissues (leaf and bud) and four species (*Q. glauca*, *Q. acuta*, *L. edulis*, and *L. glaber*). Newly flushed leaf samples are indicated as asterisks. (C–D) Hierarchical clustering of 11749 genes based on the similarity of gene expression dynamics. Daily mean temperature is shown in the top of the heatmaps.

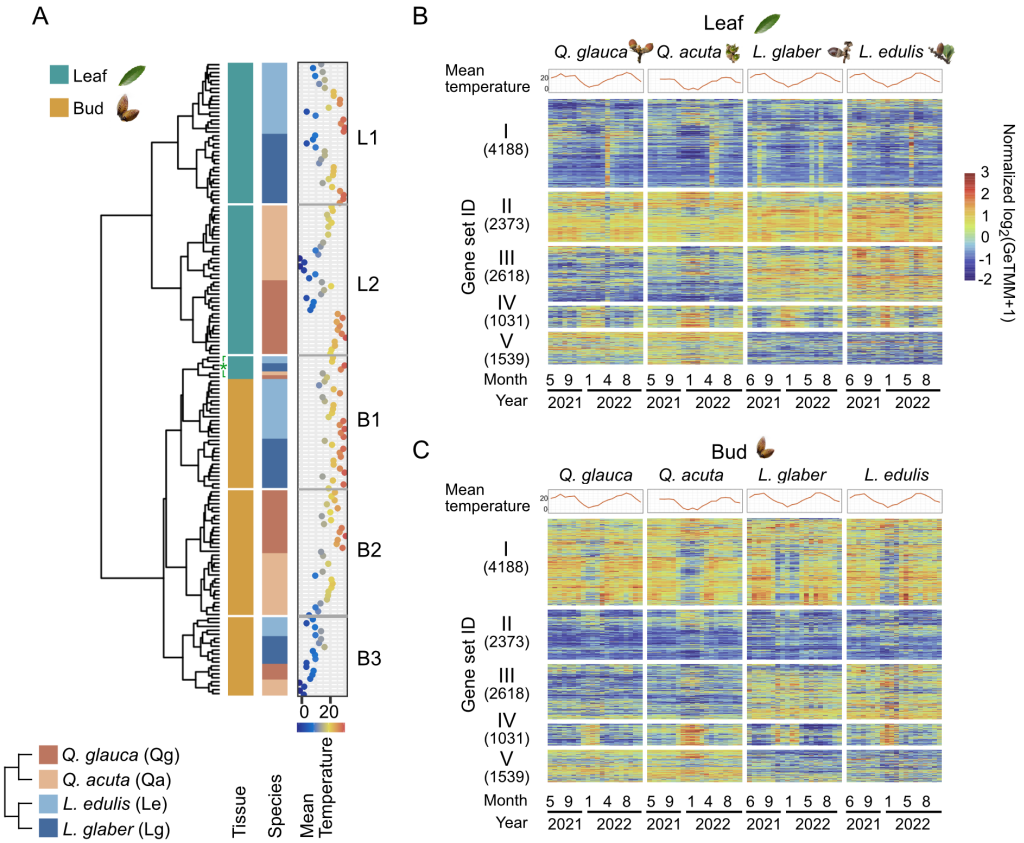

Figure S7. Seasonal gene expression dynamics under the identical environmental condition. (A) Hierarchical clustering of 161 time points from two tissues (leaf and bud) across three species (*Q. glauca*, *L. edulis*, and *L. glaber*) excluding *Q. acuta* sampled at higher elevation. Newly flushed leaf samples are indicated as asterisks. (C–D) Hierarchical clustering of 11749 genes based on the similarity of their gene expression dynamics. Daily mean temperature is shown in in the top of the heatmaps.

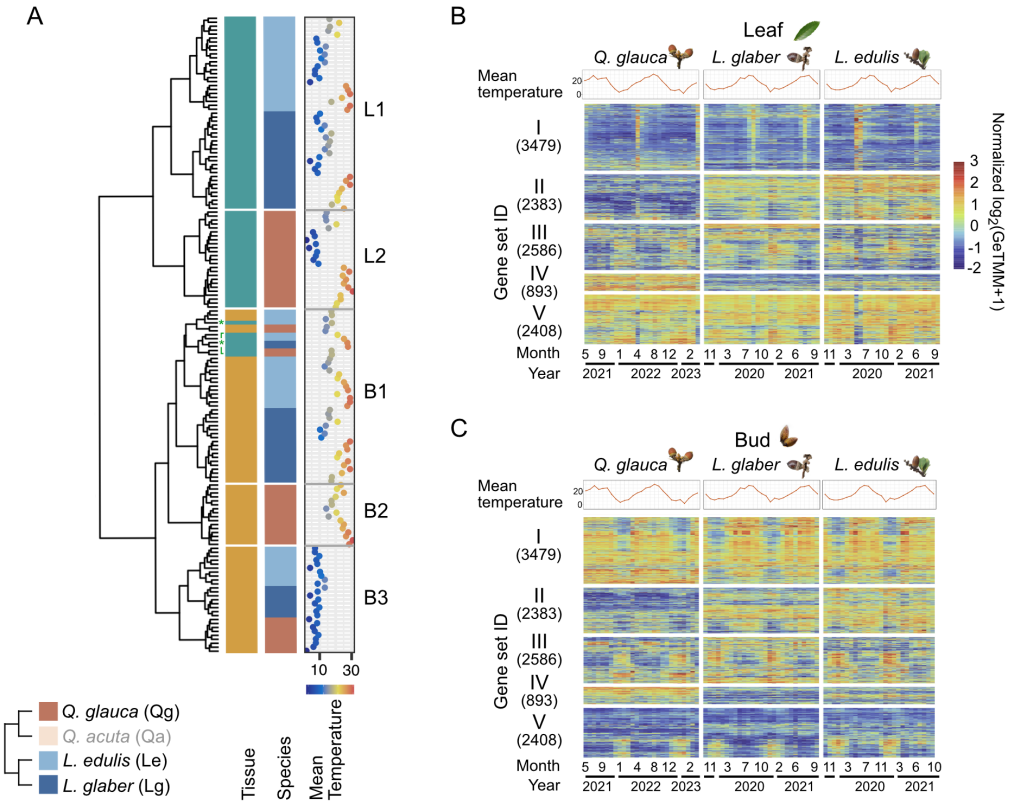

Figure S8. Distribution of environmental factors across clusters. Distribution of mean temperature for the 7 days prior to the sampling (A) and photoperiod for each sampling date (B) across clusters identified through hierarchical clustering in Fig. 2A. The Mann-Whitney U test was used to compare climatic factors between leaf clusters (L1 and L2), while the Steel-Dwass test was applied for multiple comparisons among bud clusters (B1, B2, and B3). Newly flushed leaves were included within cluster B1. Different letters denote statistically significant differences ($p < 0.05$).

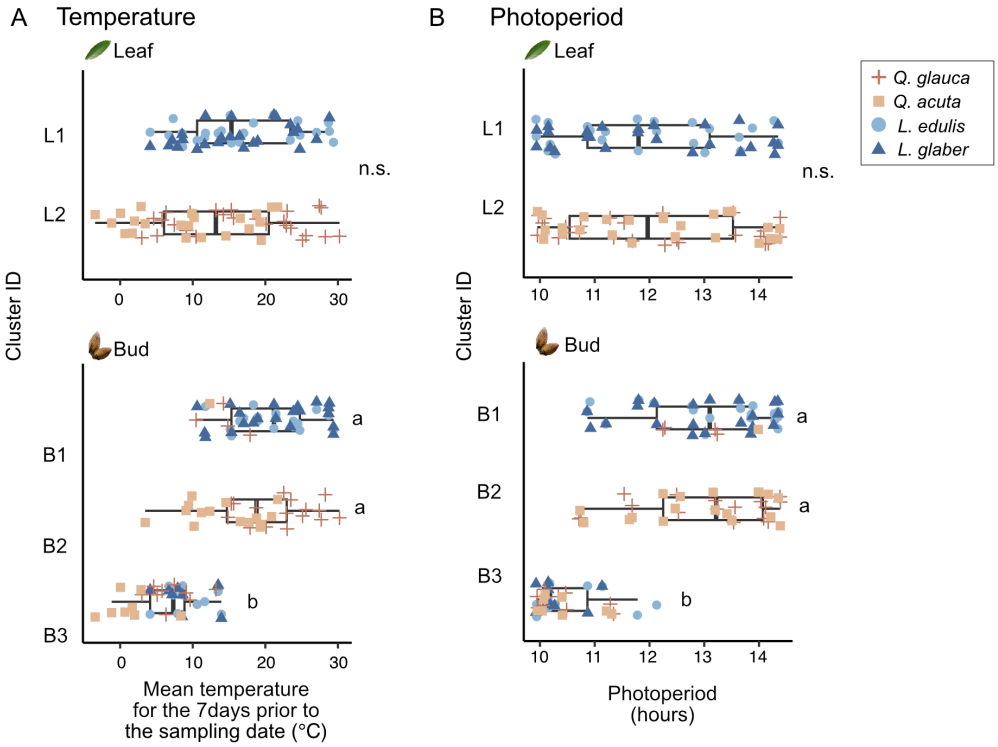

Figure S9. 3D plot of PC1–PC3 resulting from the PCA of 11749 orthologous genes in four Fagaceae species. Leaf samples are represented in a color gradient from green to blue, while bud samples range from orange to yellow. The color gradients indicate the mean temperature on the respective sampling dates for bud and leaf samples. The percentages in parentheses on each axis denote the variance explained by each principal component. The numbers within the plot indicate sampling months.

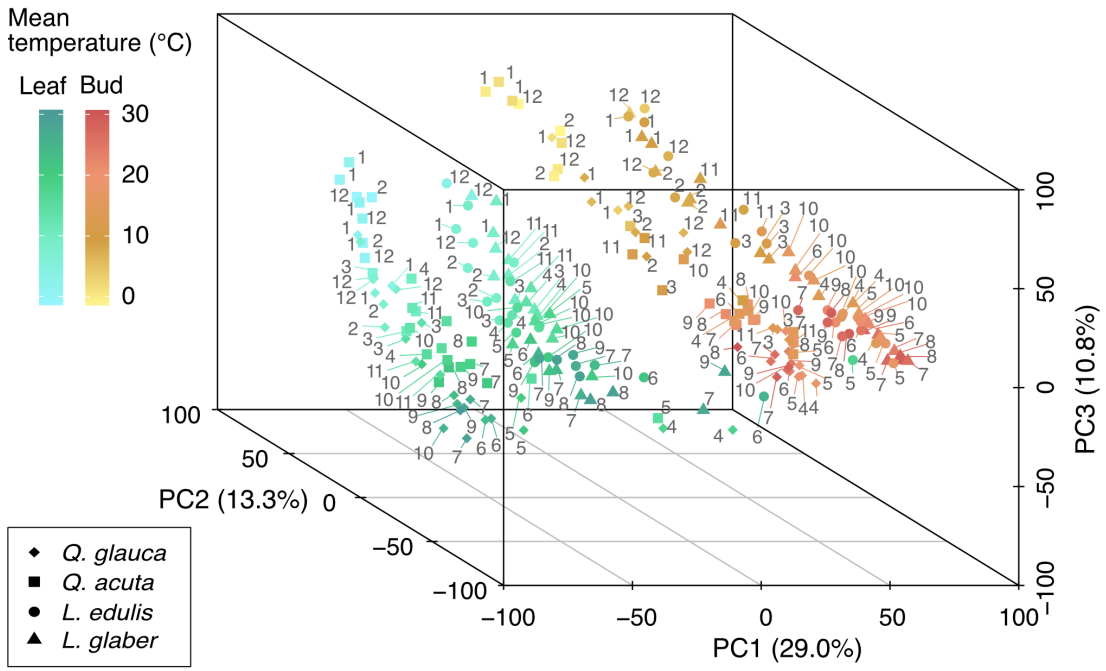

Figure S10. Number of rhythmic genes across species and distribution of peak months across half-annual genes. (A) Number of genes classified into annual (period range: 8-16 months), half-annual (< 8 month), and arrhythmic periodicity. (B–C) Number of common rhythmic genes shared among species within each species combination, categorized by annual (B) and half-annual (C) periodicity. Black dots beneath each bar indicate the species included in each combination. (D) Distribution of seasonal peaks across genes with half-annual periodicity. (E) Seasonal expression patterns of *WRKY22* in leaves and *KINγ1* in buds. For each gene, the species exhibiting a half-annual periodicity is highlighted with a thick, dark line, while the expression patterns in the other species are shown with thin, light lines.

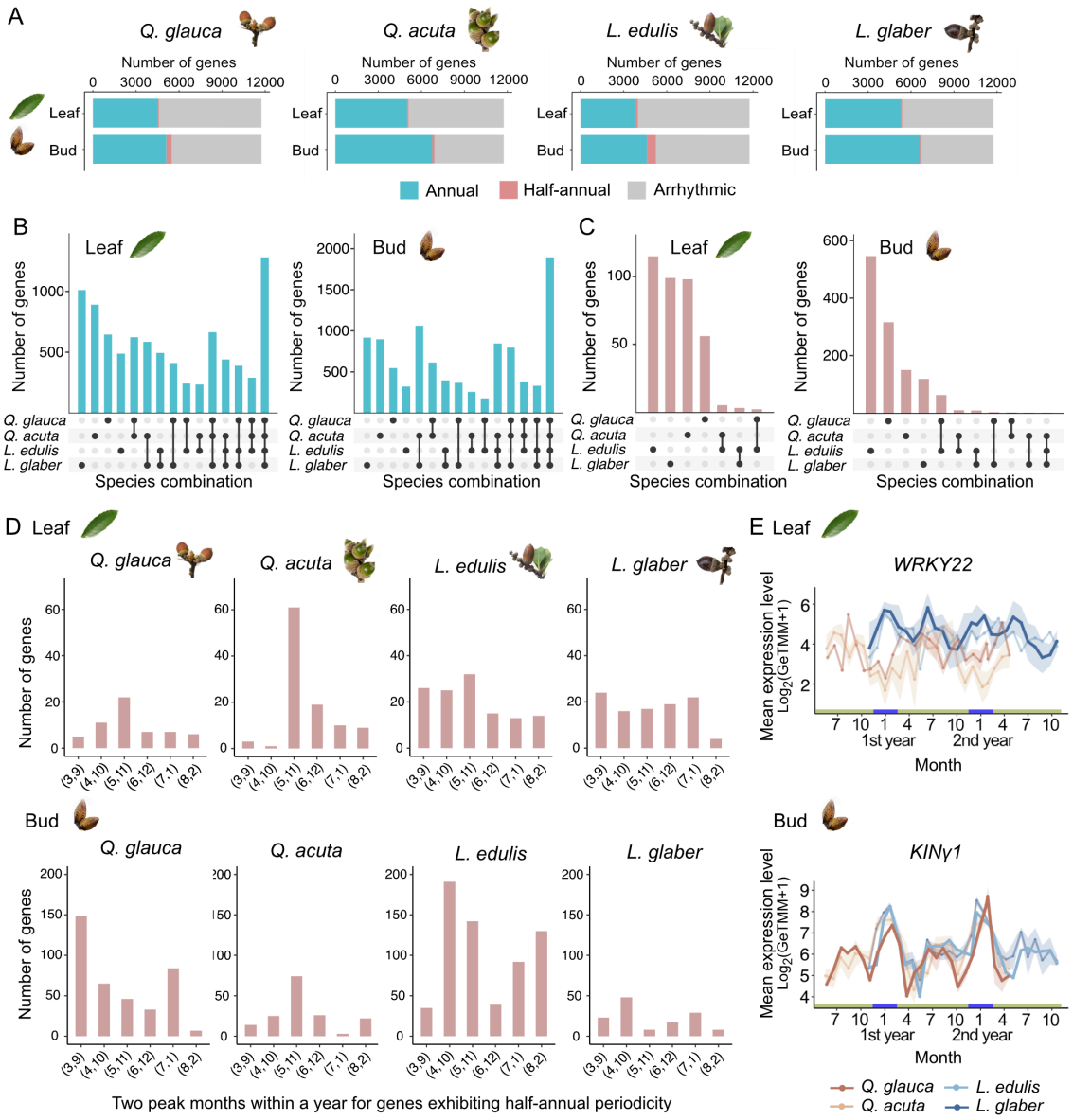

Figure S11. Comparison of peak months in seasonal gene expression across species in leaves. (A) Intra-genus and (B) inter-genera comparison of peak months in seasonal gene expression. (C) Comparison of peak months between leaves and buds. The size and color of the circles represent the number of genes and the mean of Pearson's correlation, respectively. Genes with negative correlations lower than -0.3 are highlighted in blue, while the month of leaf flushing is highlighted in green. (D) Plot of molecular phenology divergence index *D* across months. Triangles and circles indicate the *D* values calculated from intra- and inter-genera comparison, respectively. The line and shaded envelope indicate the mean and standard deviation (s.d.). Different letters denote statistically significant differences (Nemenyi test, $p < 0.05$).

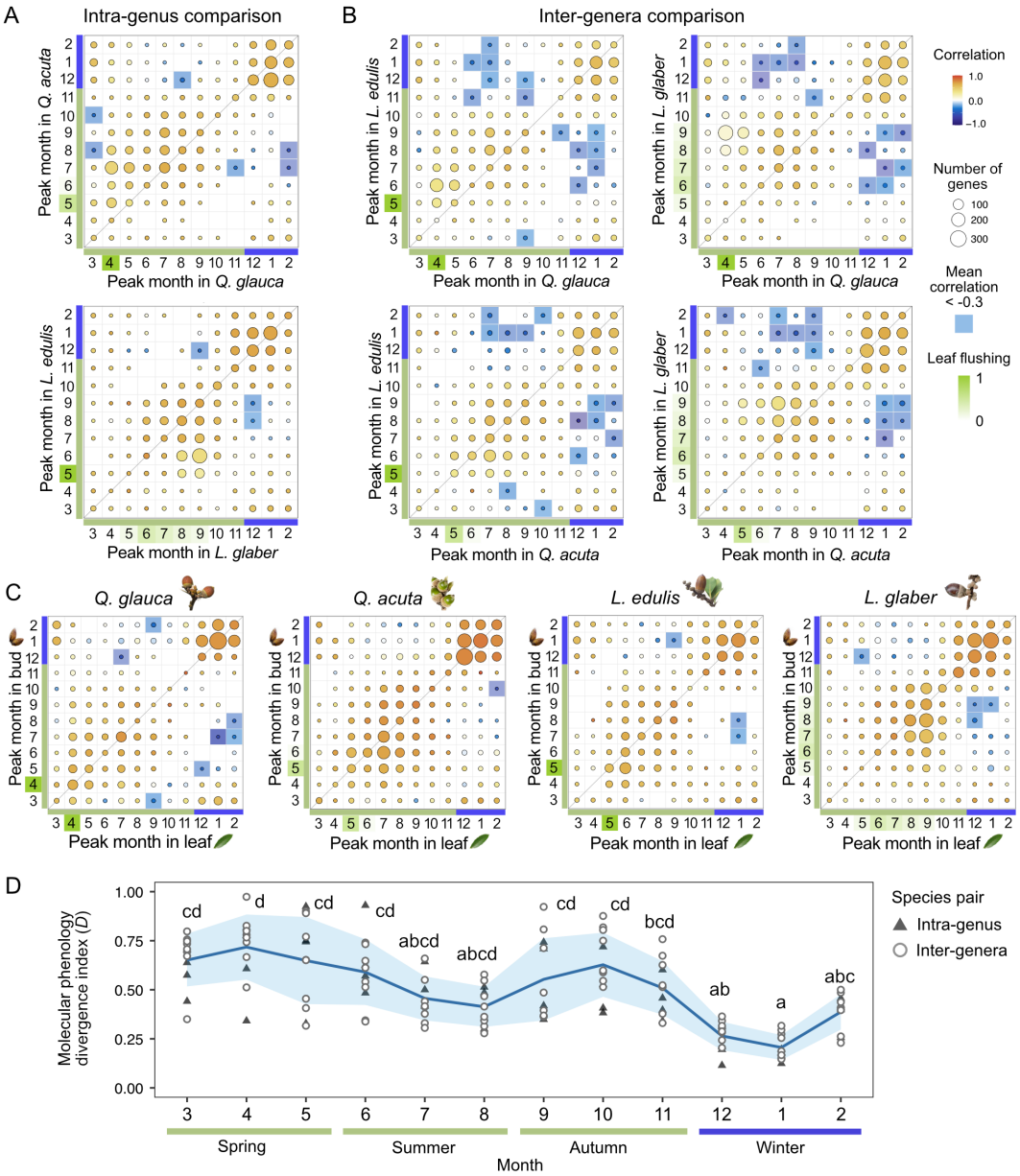

1302 **Figure S12.** Seasonal difference of molecular phenology divergence index *D*
1303 calculated for species under the identical environmental condition. Plot of
1304 molecular phenology divergence index *D* across months in buds (A) and leaves
1305 (B) calculated from the gene expression in *Q. glauca*, *L. edulis*, and *L. glaber*.
1306 Triangles and circles indicate the values of *D* calculated from intra-genus and
1307 inter-genera comparison, respectively. The line and shaded envelope indicate the
1308 mean and standard deviation (s.d.). Different letters denote statistically significant
1309 differences (Nemenyi test, $p < 0.05$).

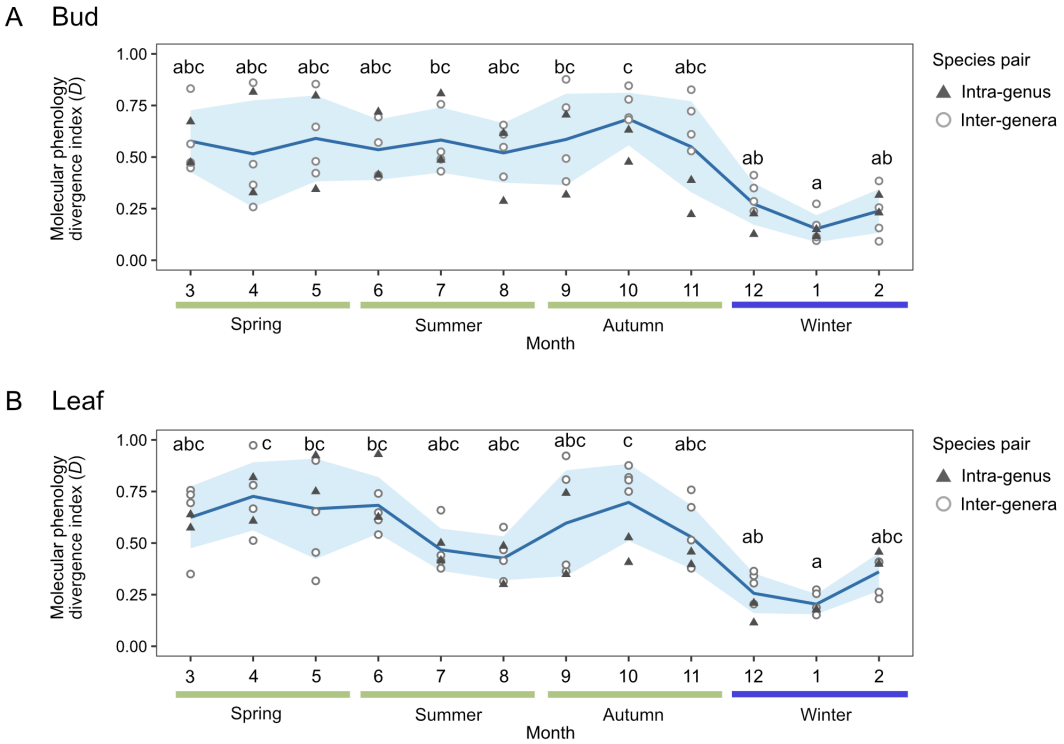

1310

1311

Figure S13 Phylogenetic constraints in the evolution of seasonal gene expression in leaves. (A) Distribution of pairwise Pearson's correlation coefficients for gene expression across species (*Le*: *L. edulis*, *Lg*: *L. glaber*, *Qg*: *Q. glauca*, *Qa*: *Q. acuta*; n = 11749). Colors indicate three categories based on the presence or absence of rhythmicity in gene expression. The median values of Pearson's correlation across all the genes were depicted as black bars. Different letters denote significantly different values (Nemenyi test, $p < 0.05$). (B) Heatmap of pairwise Pearson's correlation coefficients for each gene, along with the mean count of genes in four categories of seasonal gene expression: (1) rhythmic genes with annual periodicity peaking in the growing season (March–November), (2) rhythmic genes with annual periodicity peaking in winter (December–February), (3) rhythmic genes with half-annual periodicity, and (4) arrhythmic genes. The mean count was calculated for each block of 100 genes. Genes were ordered based on the mean Pearson's correlation of their expression across all species pairs.

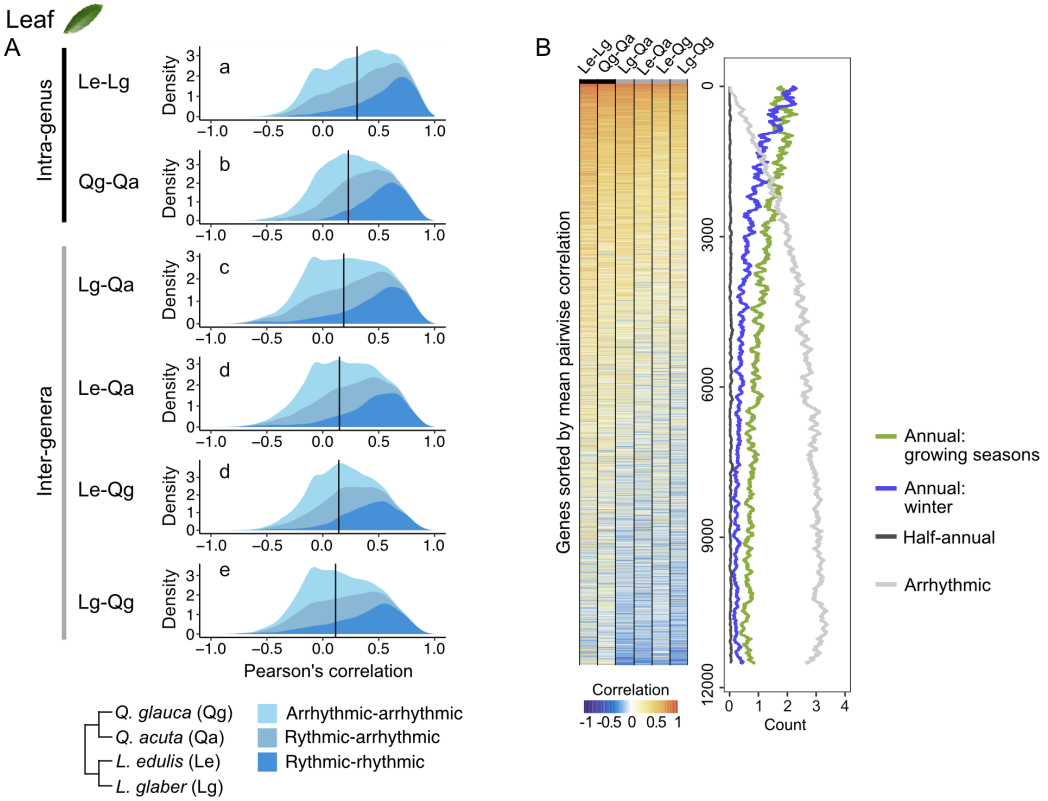

Figure S14 Distribution of pairwise Pearson's correlation coefficients for gene expression across species under the identical environmental condition. Density plot of pairwise Pearson's correlation coefficients in buds (A) and leaves (B), calculated from the gene expression in *Q. glauca*, *L. edulis*, and *L. glaber* inhabiting nearly identical environments. Colors indicate rhythmicity categories. Black bars show median correlation values, and different letters indicate significant differences (Nemenyi test, $p < 0.05$).

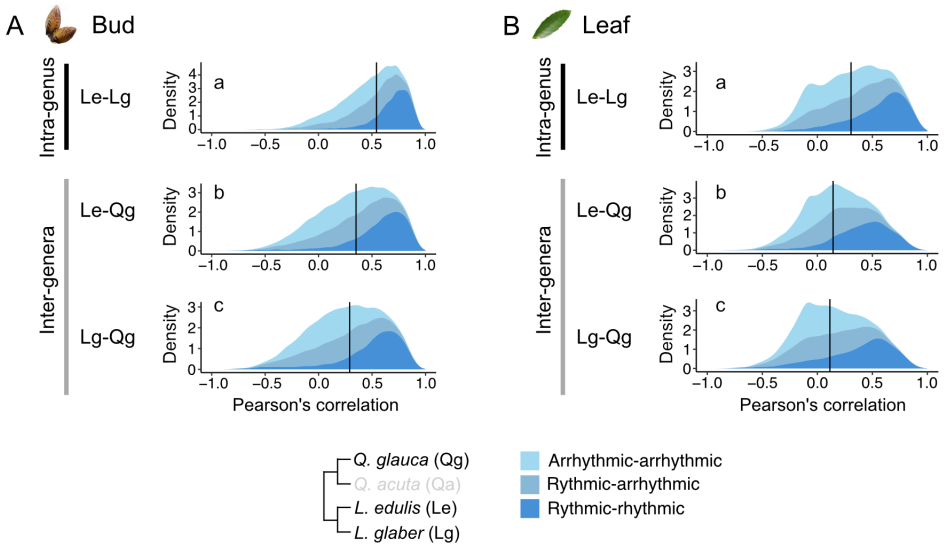

Figure S15. Pairwise mean absolute difference of gene expression dynamics. (A–B) Distribution of mean absolute difference of gene expression dynamics (Log_2(GeTMM+1)) in leaf (*A*) and bud samples (B) across species (Le: *L. edulis*, Lg: *L. glaber*, Qg: *Q. glauca*, Qa: *Q. acuta*; *n* = 11749). Colors indicate three categories based on the presence or absence of rhythmicity in gene expression. The median values across all the genes were depicted as black bars. Different letters denote significantly different values (Nemenyi test, $p < 0.05$). (C–D) Heatmap of the mean absolute difference for each gene, along with the mean count of genes in four categories of seasonal gene expression: (1) rhythmic genes with annual periodicity peaking in the growing season (March–November), (2) rhythmic genes with annual periodicity peaking in winter (December–February), (3) rhythmic genes with half-annual periodicity, and (4) arrhythmic genes. The mean count was calculated for each block of 100 genes. Genes were ordered based on the mean absolute difference of their expression across all the species pairs.

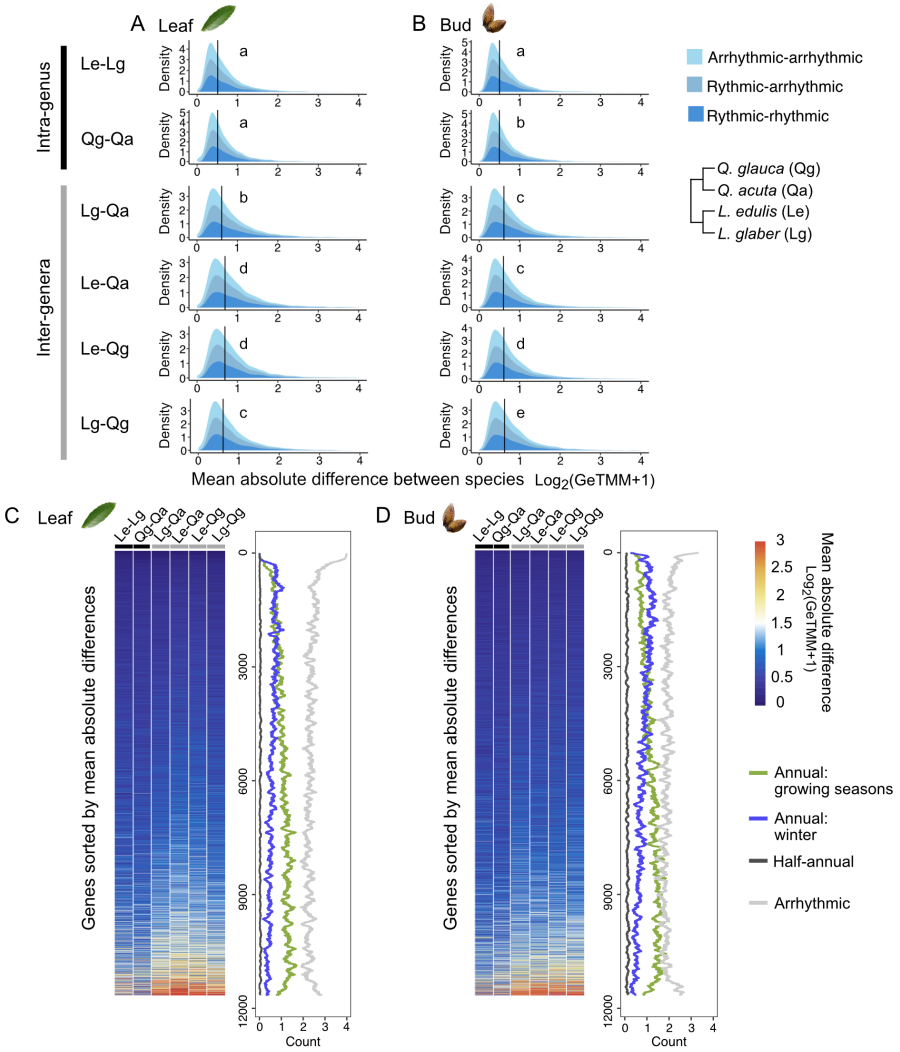

1354 **Figure S16.** Gene Ontology (GO) enrichment analysis. (A) Top 5 GO terms
1355 (ranked by the raw p-values) for the genes with conserved expression patterns
1356 across species (a mean correlation in gene expression ranking in the top 5%) in
1357 leaves and buds. (B) Top 5 GO terms for the genes with diverged expression
1358 patterns across species (a mean correlation in gene expression ranking in the
1359 bottom 5%) in leaves and buds. Genes used for the analysis are listed in Dataset
1360 S5.

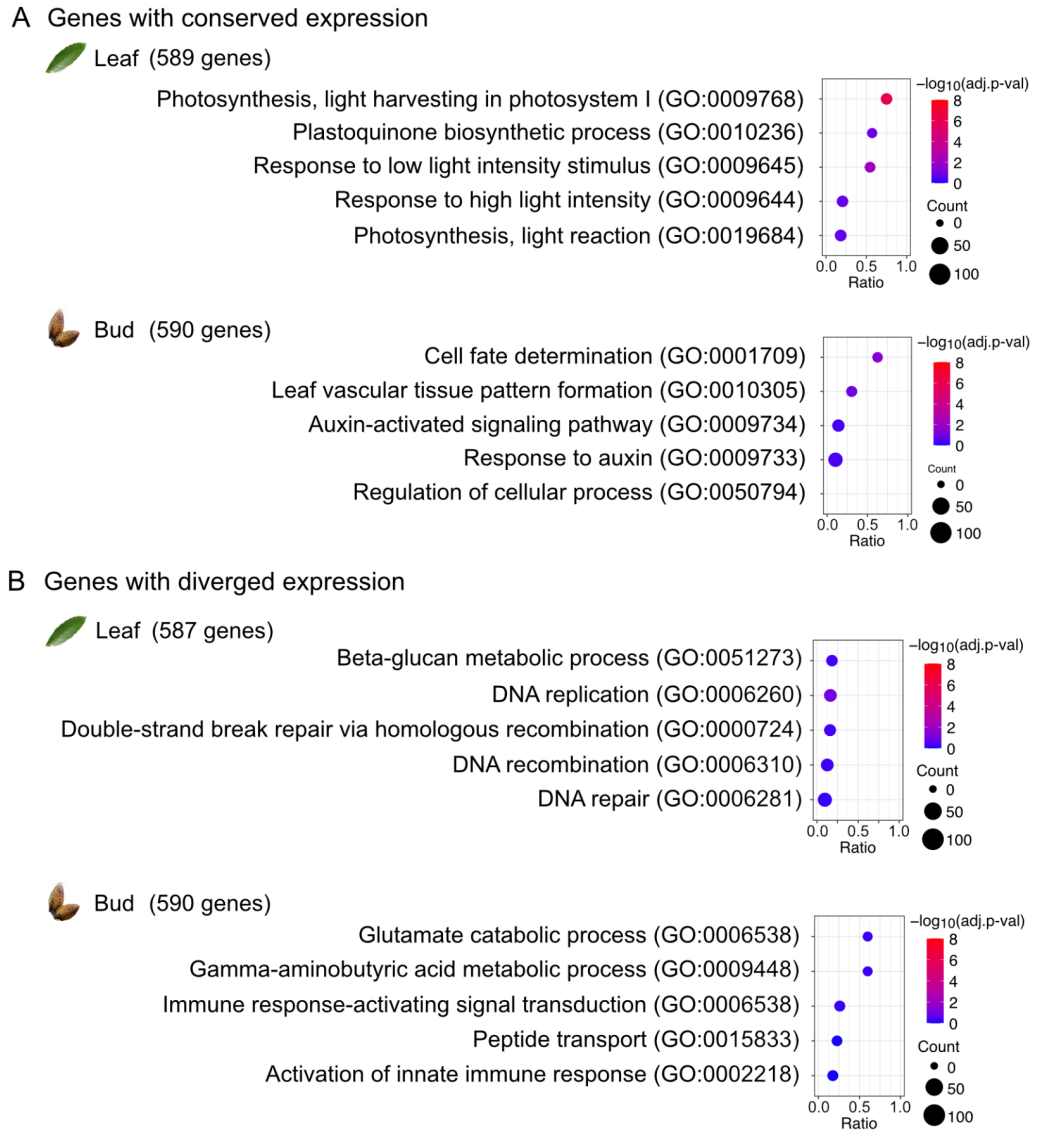

1361

1362

Figure S17. Relationship between sequence divergence and gene expression divergence. (A) Relationships between evolutionary measures (dN/dS, dN, dS), and mean expression levels of genes except for the outliers (n = 11223). (B–C) Relationships between the evolutionary measures (dN, dS) and peak differences ($\Delta\varphi$) between *Q. glauca* and *L. edulis* in leaves (B) and buds (C) using the same gene set as in Fig. 5*E* (n = 951). The regression slope and corresponding p-value are shown in each panel. Black lines and transparent bands represent regression lines and 95% confidence intervals. (D–E) Comparison of the evolutionary measures (dN/dS, dN, dS) among genes with conserved annual periodicity across four categories (n = 951). Genes were classified into four categories: those expressed in winter in both tissues, those expressed in winter only in buds, those expressed in winter only in leaves, and others. (E) shows a subset of (D), including only genes with conserved seasonal peaks (peak month difference < 2).

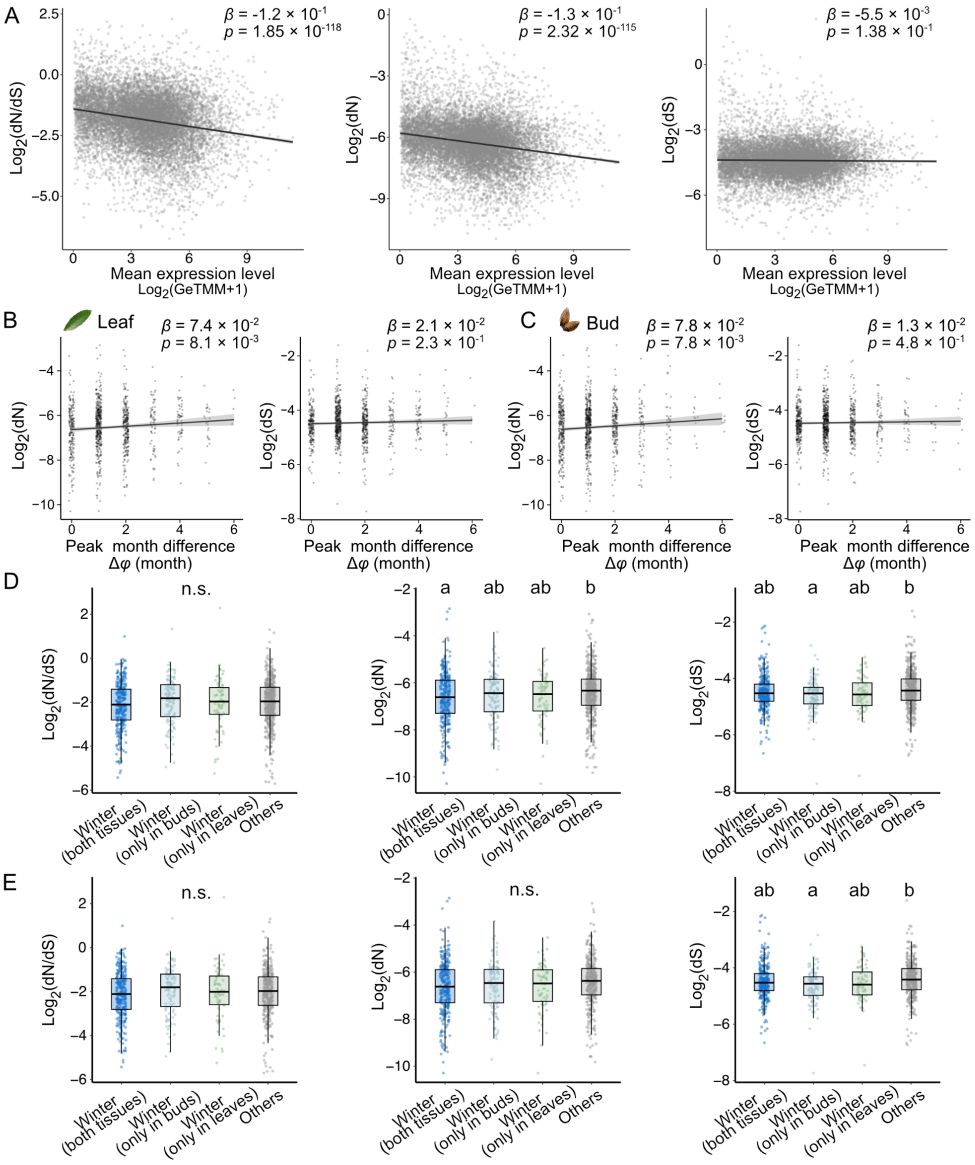

Figure S18. Developmental constraints and seasonal constraints in the evolution of gene expression. (A)The hourglass model of developmental constraints, illustrating similar gene expression during the mid-embryonic stage (40–45). (B) Seasonal constraints identified in this study. Similar gene expression patterns were observed during the winter season in both leaves and buds, as well as during the summer in leaves. The vertical axis represents time (developmental stages or seasons), while the horizontal axis represents the divergence of gene expression patterns.

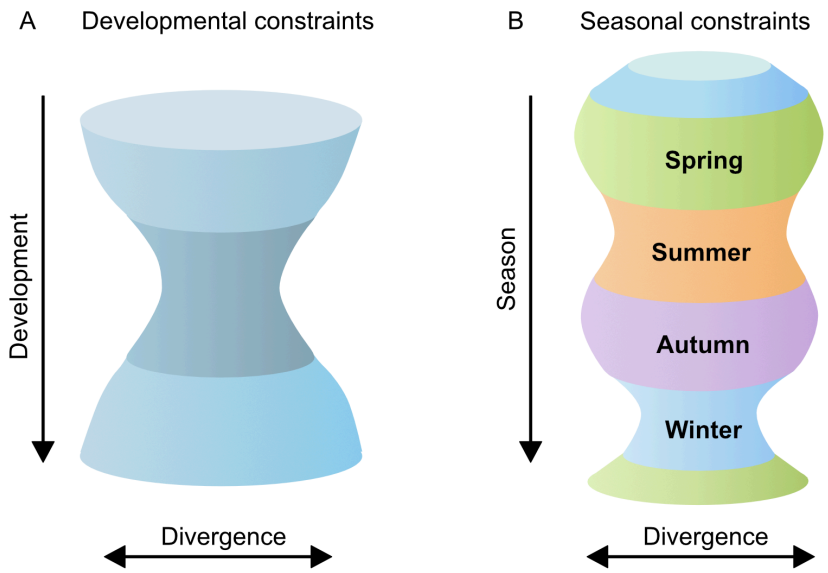

1387 **Table S1.** The statistics for genome assemblies of two new sequenced species

	Q. glauca	*L. edulis*
Sequencing		
Raw bases of PacBio (Gb)	32.6	273.6 (subreads)
Raw bases of Hi-C (Gb)	24.8	50.1
Estimated genome size (Mb)	891.2	868.7
Assembly		
Final assembly size (Mb)	867.7	835.7
Number of chromosomes	12	12
Number of contigs	797	750
N50 of contigs (Mb)	71.7	68.8
GC percent	35.68	35.74
Annotation		
Number of predicted genes	39,758	34,059
Mean gene length (bp)	3,889.70	4,099.28
Mean CDS length (bp)	1,221.90	1,164.30
Annotated to EggNOG	37,408 (94%)	31,668 (93%)

1388
1389

Other Supporting Information Files

Dataset S1
Summary of clustering 213 gene expression profiles

Dataset S2
Hierarchical clustering of 11749 gene expression dynamics

Dataset S3
Identification of genes with rhythmic expression

Dataset S4
Comparison of correlation and absolute difference among the species pairs

Dataset S5
List of genes with conserved and diverged gene expression across species.

Dataset S6
Statistical test of evolutionary rates